Chemical and textural characterisation of diagenetic to low-grade metamorphic phyllosilicates in turbidite sandstones of the South Portuguese Zone : a comparison between metapelites and sandstones

Autor(en): **Abad, Isabel / Nieto, Fernando / Velilla, Nicolás**

Objekttyp: **Article**

Zeitschrift: **Schweizerische mineralogische und petrographische Mitteilungen = Bulletin suisse de minéralogie et pétrographie**

Band (Jahr): **82 (2002)**

Heft 2: **Diagenesis and Low-Grade Metamorphism**

PDF erstellt am: **21.07.2024**

Persistenter Link: https://doi.org/10.5169/seals-62367

SCHWEIZ. MINERAL. PETROGR. MITT. 82, 303–324, 2002

Chemical and textural characterisation of diagenetic to low-grade metamorphic phyllosilicates in turbidite sandstones of the South Portuguese Zone: A comparison between metapelites and sandstones

by *Isabel Abad*[1], *Fernando Nieto*[2] and *Nicolás Velilla*[3]

Abstract

The intercalation at the meter scale of shales and sandstones in the incipient metamorphic sequence of the South Portuguese Zone allows to compare the evolution from diagenesis to low metamorphic grade in both of these lithologies. Data from X-ray diffraction, optical, scanning and transmission electron microscopy as well as whole-rock chemical analysis from the sandstones have been obtained and are compared with previously published data from the shales. Obvious textural differences are present from the outcrop scale to the low-magnification TEM scale; phyllosilicate packets in sandstones are clearly randomly oriented, with high-angle boundaries contrasting with the usual sub-parallel orientation in shales. But no differences have been found between the phyllosilicates of the two rocks types when comparing lattice-fringe images, polytypes, chemical composition or crystalline-domain size. Consequently, illite crystallinity and traditional crystal-chemical parameters, such as d_{001} and *b* cell dimension of K-white mica, produce equivalent and inter-changeable information between the sandstones and shales. The chemical compositions of the phyllosilicates are characterised by a general lack of homogeneity at the sample level. The phengitic vector is mainly responsible for the scattering of compositions, with a minor influence from the illitic vector. The grain size of very low-grade metamorphic turbidite sequences such as these should not be a limiting criterion in the sampling, because samples with intermediate characteristics between metapelites and sandstones may also provide valid results.

Keywords: very low-grade metamorphism, illite crystallinity, electron microscopy, flysch, Iberian Massif.

1. Introduction

Over the past decade or more, the application of integrated TEM and XRD studies has provided evidence that clay minerals in pelitic and metapelitic rocks undergo a series of progressive mineralogical, compositional and microtextural changes at low temperatures, below 300 °C. Examples of such studies include the Gulf Coast diagenetic sequence (AHN and PEACOR, 1986), the Welsh Basin metapelitic sequence (LI et al., 1994a), the Diablo Range (DALLA TORRE et al., 1996), the Helvetic Alps (LIVI et al., 1997) and North Cornwall (WARR and NIETO, 1998). These studies integrate structural and stratigraphic data along with both XRD and TEM data on a regional scale and produce information on reaction progress in clay minerals. Although this research has been a key factor in advancing our knowledge of metapelitic rocks (MERRIMAN and PEACOR, 1999), more research is needed to compare the clay sequences subjected to nearly identical conditions but including different lithotypes (e.g. ÁRKAI et al., 2000; MATA et al., 2001; MASUDA et al., 2001).

The diagenetic history of sandstones and adjacent shales is well known in petroleum areas. But there is little knowledge of the effect of more coarse-grained lithologies on the mineralogical

[1] Departamento de Geología. Universidad de Jaén. 23071 Jaén, Spain. <miabad@ugr.es>
[2] Instituto Andaluz de Ciencias de la Tierra y Departamento de Mineralogía y Petrología, Universidad de Granada. 18002 Granada, Spain.
[3] Departamento de Mineralogía y Petrología. Facultad de Ciencias, Universidad de Granada. 18002 Granada, Spain.

changes during very low-grade metamorphism. The key important processes that influence the diagenetic growth of phyllosilicate minerals in sandstones (e.g. permeability-porosity changes during compaction, fluid-rock interaction during dewatering and dehydration reactions etc.) are different from the set of rock properties that come into play at very low-grade metamorphic conditions, for example the onset of cleavage formation processes. Whereas clay diagenesis can significantly change the physical properties of sandstones in petroleum reservoirs, as described by many authors (e.g. KANTOROWICZ, 1984; GLASMANN et al., 1989; HASZELDINE et al., 1992), the greater permeability could allow a higher fluid/sediment ratio with a consequent predominance of dissolution/neoformation processes (YAU et al., 1987), which are very important in promoting reactions towards an equilibrium state.

Sandstones are abundant in flysch sequences. There have been many studies on metapelites in these sequences, but not on coarser rocks, such as the turbidites in the English Lake District (COOPER and MOLINEUX, 1990), the lower Palaeozoic turbiditic rocks of the Southern Uplands of Scotland (KEMP et al., 1985), and the Wenlock turbidites (DIMBERLINE, 1986). Nevertheless, sandstones are of interest as they can provide more data on low-grade metamorphism. In fact, the coarser-grained sandstones facilitate SEM textural and chemical characterisation of these rocks.

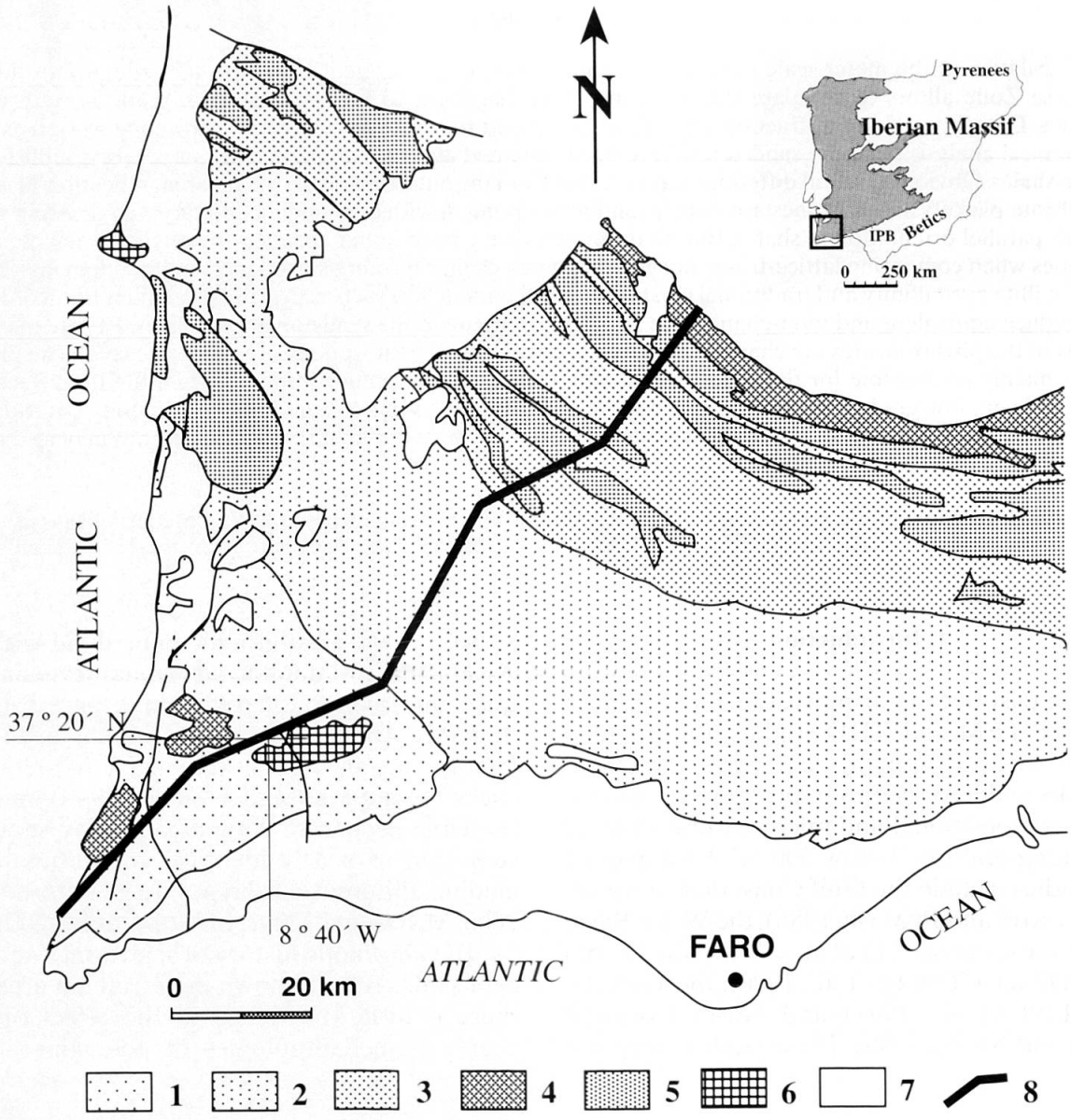

Fig. 1 Geological map of the South Portuguese Zone (adapted from OLIVEIRA, 1990 and QUESADA et al., 1991). Syn-orogenic flysch sequences of the Baixo Alentejo Flysch Group (Culm): 1—Brejeira Formation; 2—Mira Formation; 3—Mértola Formation; 4—Pre-orogenic sequences (mainly Phyllite-Quartzite Formation); 5—Volcano-Sedimentary Complex; 6—Peralkaline intrusions; 7—Meso-Cenozoic detrital cover; 8— Profile of sample location.

ABAD et al. (2001) described the metamorphic evolution of the South Portuguese Zone of the Iberian Variscan Belt, based on the metapelitic rocks found therein. They reported a progressive increase in metamorphism from diagenetic conditions in the southwest to greenschist facies conditions in the northeast. No mineral, chemical or textural data have been reported from the sandstones of these sequences, yet they are interesting for comparison of low-grade metamorphic processes in coeval sandstones and shales. The aim of this research is: (i) to determine the mineral associations and the main crystal-chemical parameters (IC, d_{001}, b) of phyllosilicates (dioctahedral mica and chlorite) by X-ray diffraction; (ii) to study the texture, structure and chemical composition of phyllosilicates using electron microscopy techniques (SEM/HRTEM) to characterise the low-grade metamorphism in sandstones from the South Portuguese Domain; and (iii) to correlate these data with results from intercalated shales (ABAD et al., 2001).

During sampling we attempted to differentiate as far as possible between metapelites and sandstones to avoid collecting rocks with intermediate characteristics. Therefore, 14 sandstone samples were selected along a SW–NE cross-section (Fig. 1) and studied by X-ray powder diffraction (XRD) and scanning electron microscopy (SEM). Based on these results, 3 samples were selected for high-resolution transmission electron microscopy (HRTEM/AEM) study.

2. Techniques

2.1. X-RAY DIFFRACTION

X-ray diffraction studies were carried out using a Philips PW 1710 powder diffractometer with Cu-Ka radiation, graphite monochromator and automatic divergence slit. The <2 μm fraction was separated by centrifugation. Oriented aggregates were prepared by sedimentation on glass slides. Ethylene-glycol and dimethyl-sulphoxide treatments were carried out on some samples to aid the identification of smectite and kaolinite, respectively. Preparation of samples and experimental conditions for illite "crystallinity" (IC) measurements were carried out according to IGCP 294 IC Working Group recommendations (KISCH, 1991). Our IC measurements (y) were transformed into C.I.S. values (x) according to the equation $y = 0.707x + 0.0034$ $(r = 0.999)$, obtained in our laboratory using the international standards of WARR and RICE (1994). IC was measured on both 10-Å and 5-Å peaks to check the effects of adjacent peaks (NIETO and SÁNCHEZ NAVAS, 1994). The b cell-parameters of micas and chlorites were obtained from the (060) peaks measured on slices of rock cut normal to the main foliation of the samples. For all the spacing measurements, quartz from the sample itself was used as internal standard.

2.2. CHEMICAL ANALYSES

Whole-rock analyses of the major elements were carried out using X-ray fluorescence (XRF) in a Philips PW 1040/10 spectrometer at the Centro de Instrumentación Científica (C.I.C.) of the Universidad de Granada. Glass beads with lithium tetraborate were employed to minimise the preferential orientation of phyllosilicates. The ignition loss (L.O.I.) was determined from 0.5 g of powdered sample, first dried at 110 °C and then heated at 1000 °C for an hour.

2.3. SCANNING ELECTRON MICROSCOPY AND HIGH-RESOLUTION TRANSMISSION ELECTRON MICROSCOPY

Following XRD investigation and optical microscopy study, carbon-coated samples were examined by SEM, using back-scattered electron (BSE) imaging and energy-dispersive X-ray (EDX) analysis to obtain textural and chemical information. These observations were performed at the Centro de Instrumentación Cientifica of the Universidad de Granada, using a Zeiss DSM 950 SEM, equipped with an X-ray Link Analytical QX-20 energy-dispersive system (EDX). An accelerating voltage of 20 kV, with a beam current of 1–2 nA and counting time of 100 s were used to analyse the phyllosilicates by SEM, using both natural and synthetic standards: albite (Na), periclase (Mg), wollastonite (Si and Ca), orthoclase (K) and synthetic Al_2O_3 (Al), Fe_2O_3 (Fe), and $MnTiO_3$ (Ti and Mn).

The structural formulae of micas were calculated on the basis of 22 negative charges $O_{10}(OH)_2$. Although these analytical techniques cannot distinguish between Fe^{3+} and Fe^{2+}, GUIDOTTI et al. (1994) showed that even in low redox parageneses, approximately 50% of Fe in muscovite is Fe^{3+} and values close to 85% can be reached in oxidizing environments. Therefore, in the formula calculations 75% of the Fe in micas is assumed to be Fe^{3+}.

Due to the very fine-grained nature of these samples, the data obtained using SEM sometimes had to be rejected because of different degrees of

contamination. When mica contamination was slight, the chlorite formula was recalculated after subtracting the contamination (determined from the K and/or Na content) from the initial analytical result to fit a new formula, based on 28 negative charges (NIETO, 1997).

After BSE examination, 3 representative specimens were selected and prepared for TEM study. HRTEM observations were obtained with a Philips CM20 (STEM) located at the C.I.C. (Universidad de Granada) and equipped with an EDAX solid-state EDX detector, operating at 200 kV, with a spatial resolution of 2.7 Å between points. This research presents results based on 79 lattice-fringe images and 51 selected-area electron diffraction (SAED) patterns.

Quantitative analyses (AEM) were obtained from thin edges using a (1000×200) Å scanning area. Counting times of 15 s and 100 s were used to minimise alkali-loss problems because short counting times improve reproducibility for these elements (K, Na) (NIETO et al., 1996). Albite, biotite, spessartine, muscovite, olivine and titanite standards were used to obtain K-factors for the transformation of intensity ratios to concentration following CLIFF and LORIMER (1975). Moreover, powders of two of the selected samples were prepared using holey C-coated Cu grids. This preparation disperses individual grains of minerals onto the grid surface. The monomineral character of each grain is checked by its electron diffraction pattern. The analyses performed on individual crystals allow a larger area to be used in the scanning transmission mode for the analysis (1×1) μm and provides better reproducibility of data due to the decrease in alkali loss. Although the powdered samples offer better analytical quality, the ion-milled samples offer textural information of the grain analysed.

3. Geological overview

3.1. SETTING

The western half of the Iberian Peninsula is occupied by the Iberian Massif, which forms part of the European Variscan Belt (small map in Fig. 1). The southernmost sector of the Iberian Massif, termed the South Portuguese Zone (SPZ), consists of Upper Palaeozoic sedimentary sequences with intercalations of acidic and basic volcanic rocks (Fig. 1). This zone has been interpreted as an exotic terrane that collided with the Ossa-Morena Zone (sector of the Iberian autochthon) during the Hercynian Orogeny (MUNHÁ et al., 1986; QUESADA, 1991, 1998; QUESADA et al., 1994). The boundary between the two zones is a typical suture zone and is exposed along a belt of Palaeozoic oceanic rocks of the Pulo do Lobo Zone and the Beja-Acebuches Ophiolite Complex (QUESADA et al., 1994) (Fig. 1).

The SPZ includes late Palaeozoic sequences comprising, from bottom to top:

(1) The Phyllite-Quartzite Formation (PQ): a platformal sedimentary formation (SCHERMERHORN, 1971) made up of alternating phyllites and quartzites, some conglomerates, and, at the top, lenses and nodules of limestone. The age of this pre-orogenic formation is Famennian (OLIVEIRA, 1990).

(2) The Volcano-Sedimentary Complex (VSC) is a heterogeneous sequence that consists of felsic to mafic volcanic rocks, shales, sandstones, jaspers and manganese ores; it hosts massive sulphide deposits (see LEISTEL et al., 1998 for a review). This complex has been dated as Upper Famenian to Middle Visean and indicates bimodal volcanic activity (SCHERMERHORN, 1971; MUNHÁ, 1983a). Sequences (1) and (2) are the main constituents of the Iberian Pyrite Belt.

(3) The Baixo Alentejo Flysch Group (OLIVEIRA et al., 1979) is composed of syn-orogenic sequences (Culm facies) of gravity-flow sediments that form a southward-prograding sedimentary cover. Three main basin formations are distinguished: Mértola, Mira, and Brejeira (OLIVEIRA et al., 1979; OLIVEIRA, 1990). These formations consist mainly of turbiditic rocks. The northernmost Mértola Formation has been dated as Upper Visean and comprises sequences of greywackes and shales with a high sandstone/shale ratio. The greywackes are feldspathic sandstones rich in rock fragments of volcanic (felsites, spilites, jaspers and rare granophyres), metamorphic (phyllites and quartzites) and sedimentary (mudstones, siltites and quartzwackes) origin. The Mira Formation is composed of several centimetre-thick beds of turbidites with low sandstone/shale ratios. The greywackes are richer in quartz than the above-described formation and contain lower amounts of volcanic rock fragments. This formation is Late Visean to Early Late Namurian in age. Finally, the Brejeira Formation, cropping out in the SW Portugal domain, is a turbiditic sequence of heterogeneous lithology, mainly comprised of dark sandstones and shales. The sandstones are mostly quartzitic and contain minor quantities of volcanic material and feldspars. The shales are decimetre-thick, greyish to bluish in colour and contain plant debris. Goniatites indicate a Middle Namurian to Lower Westphalian age for this formation (OLIVEIRA et al., 1979).

3.2. METAMORPHISM AND DEFORMATION

During the Hercynian Orogeny, the SPZ was deformed and regionally metamorphosed, with extensive cleavage formation. The most notable structural feature was the formation of an imbricate stack of thin, folded thrust sheets during a major phase of transpressional deformation related to the obduction of the Ossa-Morena Zone onto the SPZ (QUESADA, 1998).

The deformation and metamorphism in the southern part of the Iberian Massif are complex and have different characteristics in each structural domain. In the Iberian Pyrite Belt, the rocks of the Volcano-Sedimentary Complex underwent early hydrothermal metamorphism, contemporaneously with the volcanic activity, producing intense chloritization and sericitization (MUNHÁ and KERRICH, 1980; MUNHÁ, 1990; LEISTEL et al., 1998). The metamorphic grade shows abrupt changes on a decametric scale from zeolite facies to greenschist facies. Two predominant cleavages are related to the Hercynian deformation (SILVA et al., 1990; QUESADA, 1998): a local mylonitic foliation associated with shear zones and a widespread slaty cleavage related to folding. The metamorphic mineral development took place mainly during the second stage. This deformation is also the most noteworthy one in the units of the Baixo Alentejo Flysch Group, producing a slaty cleavage in pelitic rocks that becomes less penetrative towards the south.

Metamorphic zoning in the SPZ, mainly based on mineral assemblages occurring in mafic metavolcanics with some data from pelitic rocks, was established by MUNHÁ (1983b). This zoning, ranging from zeolite to greenschist facies, is in agreement with the data of ABAD et al. (2001), in which crystallite sizes measured directly from lattice-fringe images and the IC of metapelites, provide information on the evolution of the metamorphism through the sequences: decreasing IC from SW to NE. The IC values for the Brejeira and Mira Formations correspond to diagenesis and anchizone, for the Mértola and PQ Formations to high anchizone-epizone, and for the Pulo do Lobo Formation to epizonal conditions.

4. Results

4.1. PETROGRAPHY

Sampled sandstones are greywackes according to Folk's classification (FOLK, 1968). This is characteristic of sandstones from gravity-flows. Their mineral composition is relatively uniform (Table 1). All of them contain quartz, K-white mica and

Table 1 Crystal-chemical parameters and bulk mineralogy determined by XRD and SEM.

	White mica			Chlorite		Mineral Composition
	d(001)		IC <2μm	d(001)		Ms, Qtz, Ab
Samples	<2μm	bulk	10Å	<2μm	bulk	(all samples)
Brejeira Formation						
Pc–11a	9.992	9.985	0.46	–	–	Kln, Gt, Kfs
Pf–23a	10.013	10.014	0.40	–	–	Ill/Pg, Kln,Gt, Kfs, Gr
Mira Formation						
Pi–33a	9.993	9.990	0.57	14.13	14.16	Chl, Hem, Ill/Pg
Pj–39a	9.981, 9.610	9.996	0.40	14.14	13.98 *	Chl, Kln, Pg , Kfs
Pk–42a	10.008	–	0.33	14.14	–	Chl, Ill/Pg, Gt, Ilm
Pl–45a	10.000	10.003	0.37	14.14	14.13	Chl, Kln
Pm–50a	9.997	10.006	0.39	14.13	14.13	Ill/Pg, Chl, Kln, Gt, Hem
Pn–53a	10.006	9.992	0.57	–	–	Kln, Pg, Ill/Pg, Gt, Kfs
Po–57a	9.997	10.003	0.25	14.16	14.01 *	Chl
Mértola Formation						
Pp–64a	9.992, 9.613	–	0.25	14.11	–	Chl, Hem, Kln, Pg, Py
Pq–67a	10.002	–	0.25	14.02 *	–	Chl, Cc
Ps–73a	9.991	–	0.29	14.14	–	Chl
Pu–75a	9.992	–	0.26	14.15	–	Chl
PQ Formation						
Px–86a	10.004	9.993	0.34	14.08 *	14.04 *	Chl, Gt, Kln, Kfs

Mineral abbreviations according to KRETZ (1983). Ill/Pg — intermediate Na-K mica. In bold, samples studied by TEM. * indicates chl basal-spacings slightly low and with significant differences among (003), (004) and (005) measures.

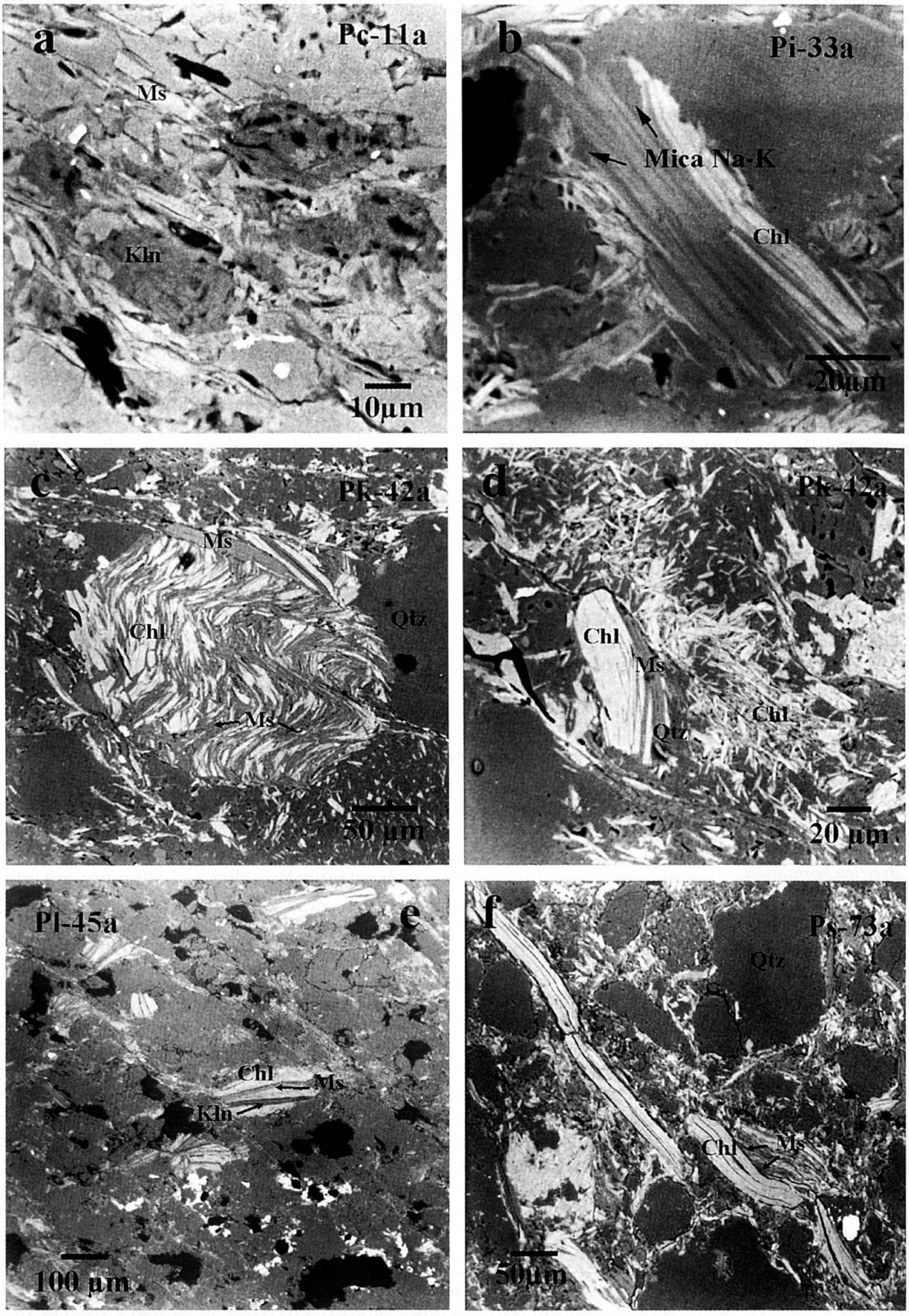
a
Pc-11a
Ms
Kln
10μm
b
Pi-33a
Mica Na-K
Chl
20μm
c
Pk-42a
Ms
Chl
Qtz
Ms
50 μm
d
Pk-42a
Chl
Ms
Chl
Qtz
20 μm
Pl-45a
e
Chl
Ms
Kln
100 μm
f
Ps-73a
Qtz
Chl
Ms
50μm

Fig. 2

feldspars. In addition, intermediate Na-K micas occur in the Brejeira and Mira Formations sometimes with paragonite. Significant amounts of chlorite and kaolinite have also been detected in several samples. Accessory minerals include goethite, hematite, graphite and ilmenite.

The samples are predominantly medium- to coarse-grained, and the fabrics are very similar. Generally, these rocks are homogeneous, comprising a framework of angular quartz grains and phyllosilicate intergrowths (Figs. 2a–f) formed of crystals stacked along the c-axis, up to 50 μm in thickness (Fig. 2). The quartz grains range from tens to hundreds of μm in diameter and the stacks up to 200–300 μm in length. The matrix is very fine-grained (<5 μm) and mainly composed of phyllosilicates and reddish Fe-oxides, responsible for the brown colour of almost all the samples.

The presence of chlorite-mica intergrowths is common in most of the sandstones sampled. They have been described in the literature mainly from metapelites in the anchizone (MILODOWSKI and ZALASIEWICZ, 1991; LI et al., 1994b) and also in fine-grained turbidite sandstones (DIMBERLINE, 1986) and quartz-arenite facies (GIORGETTI et al., 1997). In the studied samples, these stacks show differences from one sample to another, mainly in size, morphology and mineral composition (Figs. 2a–f). Generally, they consist of Fe-rich chlorite and white mica and sometimes of chlorite-mica-kaolinite or very elongated prismatic mica and chlorite crystals (Fig. 2f). Most packets are intergrown subparallel to (001), some grow as wedges, forming semi-coherent boundaries with neighbouring crystals. In some cases they are elongated, but there are ellipsoidal and equidimensional stacks as well. Their borders are often curved and frequently oriented at a low angle to the mineral cleavage (Fig. 2e); they often retain textures that suggest a detrital origin (Fig. 2c). The prismatic crystals and the stack orientation are normally coherent, but in some sandstones 'cross-like' fabrics have been observed, such as those described by MILODOWSKI and ZALASIEWICZ (1991) in the Llandovery mudrocks of Wales. Chlorite is normally the major phase, as in other sequences (DIMBERLINE, 1986; GIORGETTI et al., 1997), whereas white mica is more poorly developed and appears within chlorite (Fig. 2d). Such stacks, though smaller, have also been reported in the Mira Formation metapelites (ABAD et al., 2001, Fig. 4A).

4.2. CRYSTAL-CHEMICAL PARAMETERS

The basal spacing of mica (d_{001}) is around 10 Å, with a standard deviation of (σ) < 0.01 (Table 1). In chlorite, the basal spacing shows, in a few cases, slight differences not only between the <2 μm fraction and the bulk fraction (Table 1, d_{001} values with asterisk), but also among the (003), (004) and (005) peaks.

Figure 3 portrays the IC values for both sandstone and pelite lithologies across the region, which reveal a stepwise increase in metamorphic grade from typical late diagenetic-low anchizone values in the Brejeira and Mira Formations to high anchizone-epizone conditions in the Mértola and Phyllite Quartzite Formations. The Brejeira and Mira Formation samples show a notable difference (≈0.1 $\Delta°2\theta$) between the IC values corresponding to bulk-rock samples and the <2 μm fractions, although close to the Mértola Formation these differences decrease and, in fact, almost disappear. Some of the Mira Formation sandstones have high IC values caused by the presence of other phyllosilicates such as paragonite and/or Na-K mica, whose (001) peaks are superimposed to 10 Å peaks. Although the coincidence of 10 and 9.6 Å peaks of these mineral phases invalidate the IC data, they do indicate the metamorphic grade.

An average value of 8.99 Å (σ = 0.01) was obtained for the *b* parameter of K-white mica. As white mica is much less abundant in the sandstones than in the interbedded shales, the measurement of the *b* parameter was difficult in most of the sandstones.

4.3. CHEMICAL BULK COMPOSITION

Chemical analyses of the major elements of sandstones are given in Table 2. Although the lithologies are different, it is interesting to compare these data with the average of Post-Archean Australian Shales (PAAS) published by TAYLOR and MCLENNAN (1985) and commonly used as reference shales. As expected the sandstones are richer in Si and poorer in Al than the standard shales (PAAS) and coeval metapelitic rocks (ABAD et al., 2001). The K content and, specially, the Ca content are lower than in the PAAS. By contrast, the amount of Na is higher than in the average shales. But, in general, no significant differences

←*Fig. 2* Back-scattered electron images showing the various textures of the samples. (a) Textural appearance of sandstone Pc-11a. (b) Stack formed of chlorite and Na-K micas in sandstone Pi-33a. (c) and (d) Different types of stacks in Pk-42a, comprising mica and chlorite, the stack studied by TEM is the same type as in (d). (e) Crenulation foliation affecting stack morphology, which are re-oriented and fusiform. (f) Framework and matrix of Ps-73a. Abbreviations according to KRETZ (1983), Ill/Pg — intermediate Na-K mica.

have been detected. The only noteworthy feature detected among the formations is that the Fe and Mg contents are lower in Brejeira Formation than in the others (Table 2, samples Pc-11a and Pf-23a).

4.4. TEM OBSERVATIONS

Based on XRD and SEM data, three sandstones representative of the various geological zones of this sequence were chosen for HRTEM study of the phyllosilicates: Pc-11a (Brejeira Formation), Pk-42a (Mira Formation) and Px-86a (Phyllite-Quartzite Formation). The three samples are close to Pc-9, Pk-43 and Px-81 respectively (see Fig. 3), that is, the corresponding metapelitic rocks previously studied by HRTEM by ABAD et al. (2001).

Late diagenetic sandstone **Pc-11a** is mainly composed of dioctahedral mica and kaolinite. They are frequently intergrown (Fig. 4), with both parallel and contact-angle boundaries. The kaolinite appears to be defect-rich, with layer terminations and apparent basal slip surfaces that generate fissures. The packets are >300 Å thick. The dioctahedral mica, almost defect-free and with a 2M polytype (Fig. 4 inset), shows a more crystalline aspect and is thicker than the kaolinite.

Anchizonal sandstone **Pk-42a** is characterised by a coarser grain size and contains mica-chlorite stacks of different morphologies. At the nanoscale, the matrix is dominated by packets of white mica and chlorite, in some cases exceeding several thousand ångstroms in thickness. However, there are also subparallel packets of no more than 10–12 layers with 10-Å periodicity. Texturally, the images commonly show frequently elongated, narrow fissures, strain-related defects (e.g. contrast changes normal to the lattice fringes) and layer terminations (Fig. 5). Some SAED patterns indi-

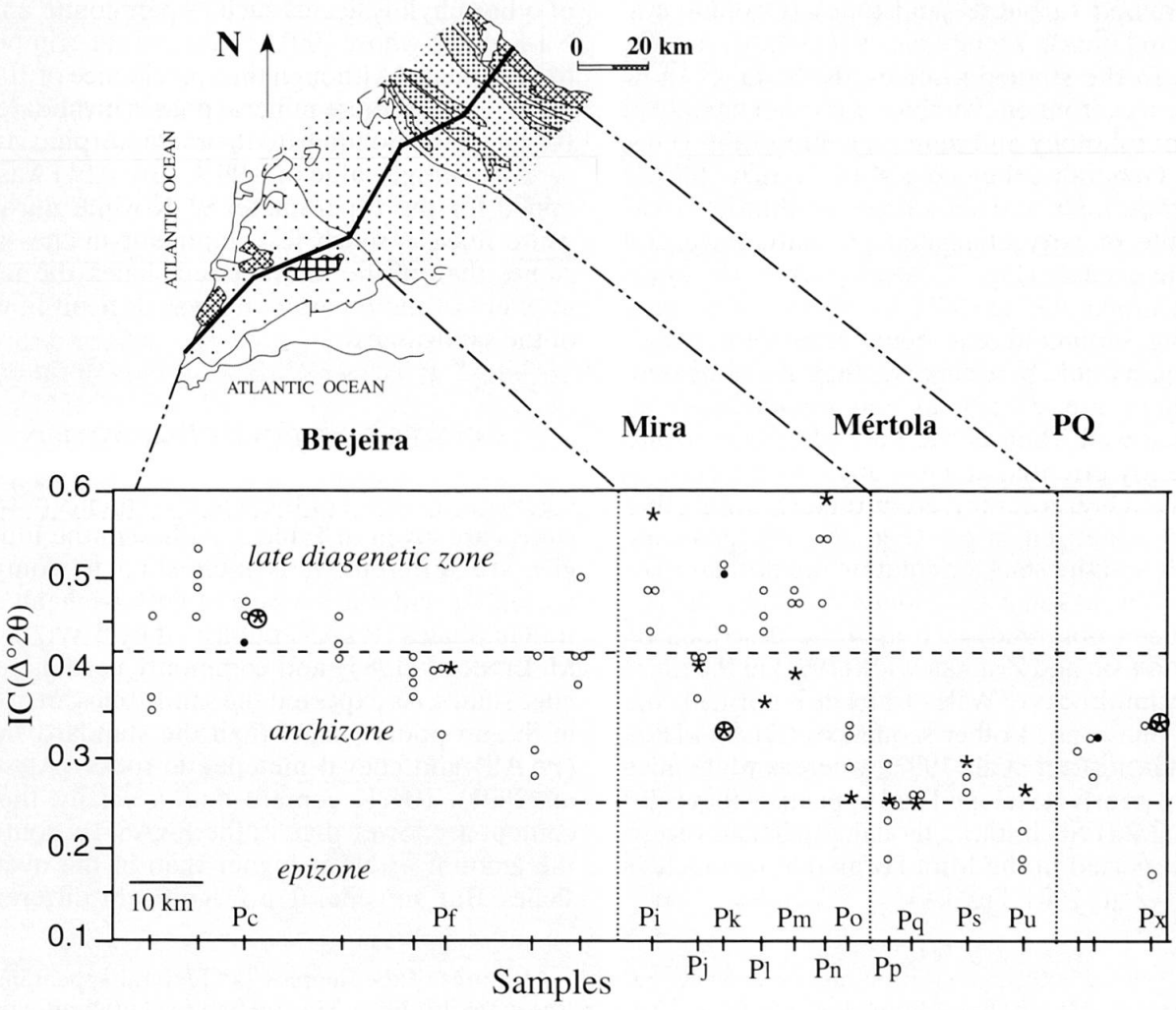

Fig. 3 Illite crystallinity (IC) of the studied samples, in relation to their geological and sample locations (*—sandstones, ○—metapelites). PQ—Phyllite-Quarzite Fm. Samples studied by TEM: circled *—sandstones; •—metapelites). Data for metapelites are from ABAD et al. (2001).

cate dominant chlorite (14-Å periodicity) with streaking along c*, consistent with the presence of layers of variable spacing observed in the lattice-fringe images (Fig. 6).

We prepared a thinned ion-milled grid of one of the mica-chlorite stacks of sample Pk-42a (see Fig. 2d) to characterise its texture, polytypism and chemical composition at the nano-scale. The results are similar to those for the matrix phyllosilicates. The mica is a 2M polytype, whereas the chlorite consists of ordered or semi-random polytypes. Packet size is around several hundred ångstroms. In addition, the mica-chlorite relation of the stacks found at SEM scale (see petrography section) is repeated at the nano-scale, where the mica and chlorite packets have sub-parallel or low-angle boundaries with one included within the other (Fig. 7). However, these relations were not found in the TEM images from the matrix.

Anchizonal sandstone **Px-86a**, in addition to having clearly metamorphic minerals (white mica and chlorite), also contains kaolinite, a mineral of lower metamorphic grade.

Texturally (Fig. 8a), the lattice-fringe images reveal thick chlorite packets (several thousand ångstroms) with subparallel, and, in some cases, high-angle crystal-boundaries (Fig. 8b), showing contrast and fine fissuring. As in sample Pk-42a, the electron diffraction spots are commonly streaked parallel to c* axis, very evident for l=2 reflections (Fig. 9). In both cases, the AEM microanalyses of these domains show them to be particularly poor in octahedral cations (values of ≈5.5 a.f.u.), although in sample Px-86a there is a slight contamination by K (≈0.15 a.f.u.). The mica crystals are also thick and we have found high-angle relations with chlorite crystals. In these images there are deformation-induced features (e.g. wavy lattice-fringes) and layer terminations, both in mica and chlorite (Fig. 9), that also suggest that lattice strain has not recovered during metamorphism. Finally, we have seen superperiodicities of up to 70-Å in the micas, revealing a long-range stacking order (Fig. 10, inset). This lattice-fringe image shows the intercalation of 7-Å kaolinite layers in a large packet dominated by muscovite layers (Fig. 10).

The measurements taken directly from the lattice-fringe images for the thickness of the mica packets give values very similar for all of the three samples, on the order of hundreds of ångstroms, only rarely exceeding 1000 Å.

The X-ray diffractograms do not reveal the periodicities detected for samples Pk-42a and Px-86a in the TEM lattice-fringe images of chlorite, as for example minor 10-Å layers in 14-Å packets or areas showing 24-Å periodicities. However, in a few cases (Table 1), chlorite basal spacings are slightly low (<14.1 Å). Therefore, we assume that those periodicities are present in several samples indicating lower periodicities than the 14-Å layer of chlorite.

4.5. CHEMICAL COMPOSITIONS OF PHYLLOSILICATES

The chemical compositions of the sandstone phyllosilicates were determined by EDX on the SEM. In addition, grids were prepared from samples Pc-11a and Px-86a in order to characterise the compositions of white mica in the TEM and thus directly compare these data with those of the coeval metapelites, avoiding instrument-derived differences.

Table 2 Whole-rock analyses of major elements of sandstones (oxide weight %).

Samples	SiO_2	TiO_2	Al_2O_3	Fe_2O_3	MnO	MgO	CaO	Na_2O	K_2O	P_2O_5	L.O.I.
Pc-11a	79.90	0.81	12.45	0.94	0.00	0.18	0.04	0.26	1.29	0.11	3.85
Pf-23a	76.67	0.90	14.01	1.55	0.00	0.21	0.02	0.32	2.12	0.05	3.98
Pi-33a	70.67	0.74	11.48	8.90	0.25	1.69	0.04	0.97	1.19	0.11	3.58
Pj-39a	72.93	0.88	13.55	4.14	0.02	0.94	0.02	1.33	1.84	0.06	4.02
Pk-42a	69.80	0.78	14.01	6.26	0.06	1.65	0.13	1.65	1.77	0.12	3.43
Pl-45a	74.04	0.92	12.04	5.66	0.04	1.13	0.05	1.04	1.55	0.10	3.04
Pm-50a	71.89	0.75	12.68	7.24	0.11	1.80	0.04	1.13	1.20	0.09	3.34
Pn-53a	67.33	0.99	17.61	5.09	0.06	0.35	0.04	0.74	2.47	0.12	5.00
Po-57a	69.07	0.77	13.98	6.60	0.09	1.67	0.22	2.15	1.40	0.15	3.64
Pp-64a	63.86	0.77	16.29	6.78	0.07	1.85	0.09	1.87	2.14	0.05	5.88
Pq-67a	65.40	0.74	14.76	5.99	0.11	1.87	1.61	3.53	1.85	0.14	3.84
Ps-73a	61.84	0.88	18.21	7.28	0.09	2.30	0.31	2.10	2.78	0.15	3.83
Pu-75a	69.82	1.00	13.89	6.10	0.08	1.53	0.33	2.68	1.45	0.14	2.71
Px-86a	72.48	0.85	12.55	6.34	0.03	1.25	0.18	0.83	1.65	0.15	3.64

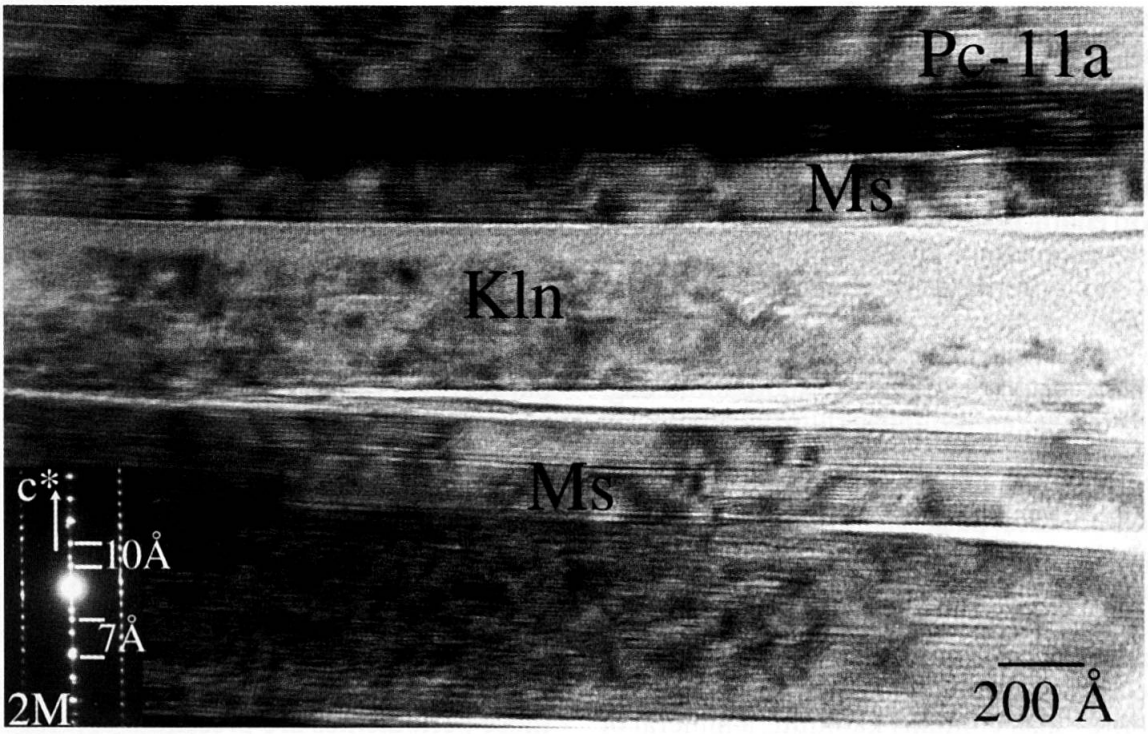

Fig. 4 Lattice-fringe image showing the relationship between white mica and kaolinite. The SAED reveals the reflections of both phases. The beam damage is obvious in the kaolinite packets.

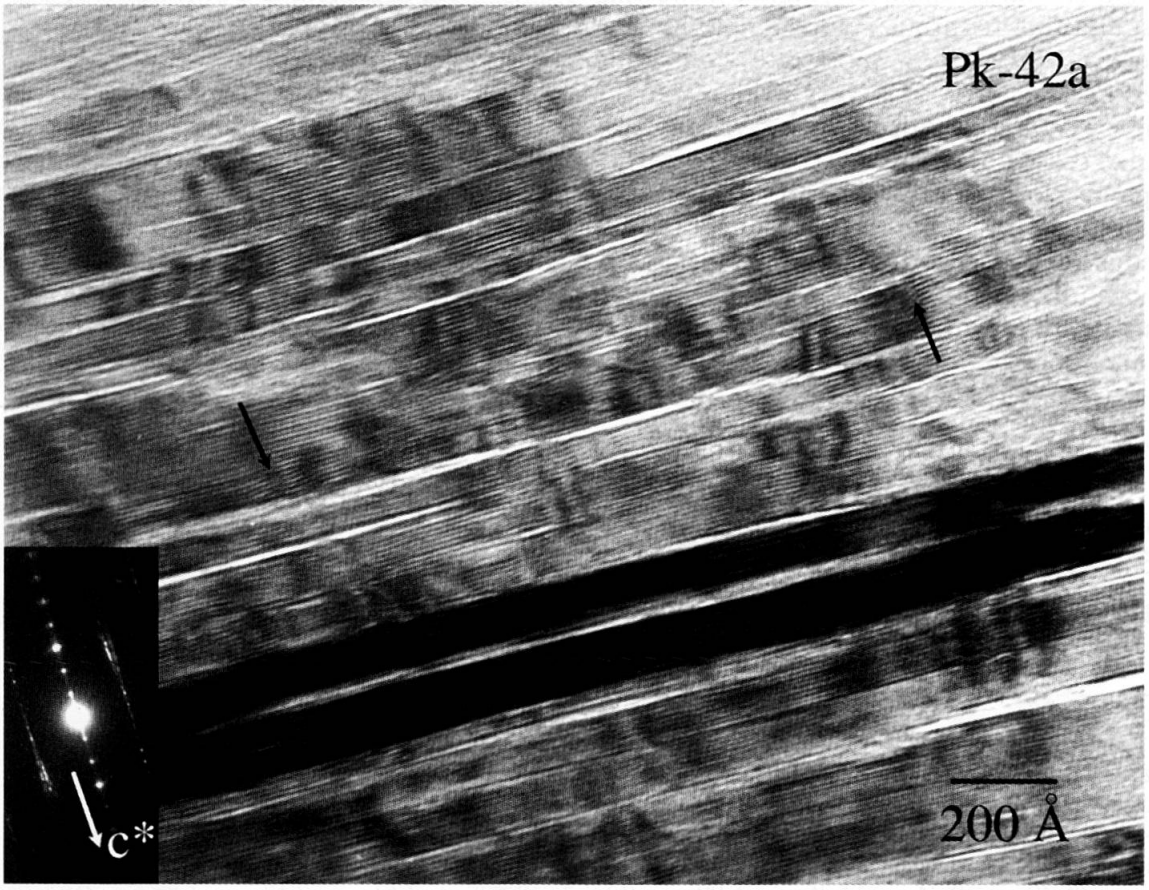

Fig. 5 Lattice-fringe image of mica crystals having similar contents of Na and K, with common wavy layers (left arrow) and layer terminations (right arrow). This texture seems to indicate incipient strain. This photo is very similar to Fig. 5 in ABAD et al. (2001) corresponding to a pelite of the same grade.

Fig. 6 Lattice-fringe image of chlorite crystals having lower periodicities (e.g. 7-Å), layer terminations (left arrow) and narrow voids affecting only one layer (e.g. right arrow). In the upper left 24-Å layers have been detected. The SAED, with 14-Å periodicity, shows streaking along c*.

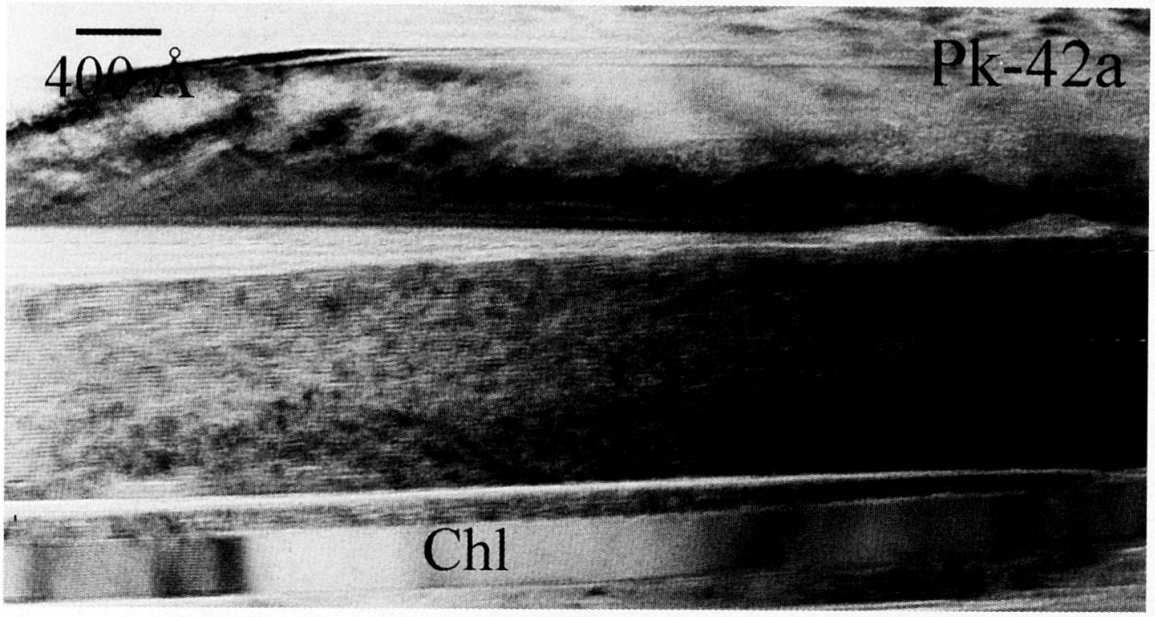

Fig. 7 Lattice-fringe image showing a detail of a chlorite-mica stack in which a defect-free chlorite packet of 20 layers is located within thick mica packets.

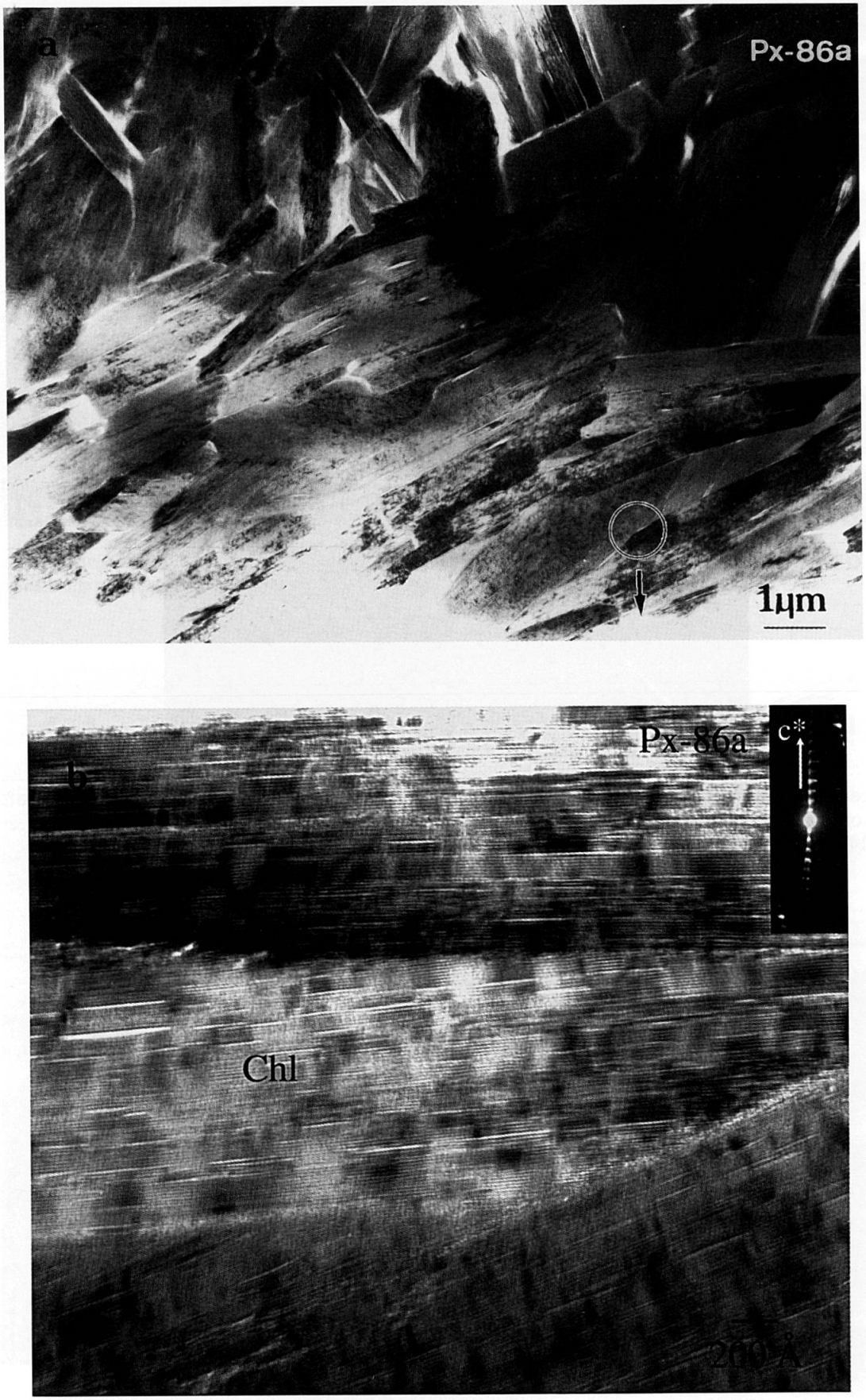

Fig. 8 (a) Low-magnification image that illustrates the general texture of a mainly phyllosilicate area. (b) Enlarged area that shows the relationships among chlorite crystals with evident contrasts and very narrow fissures.

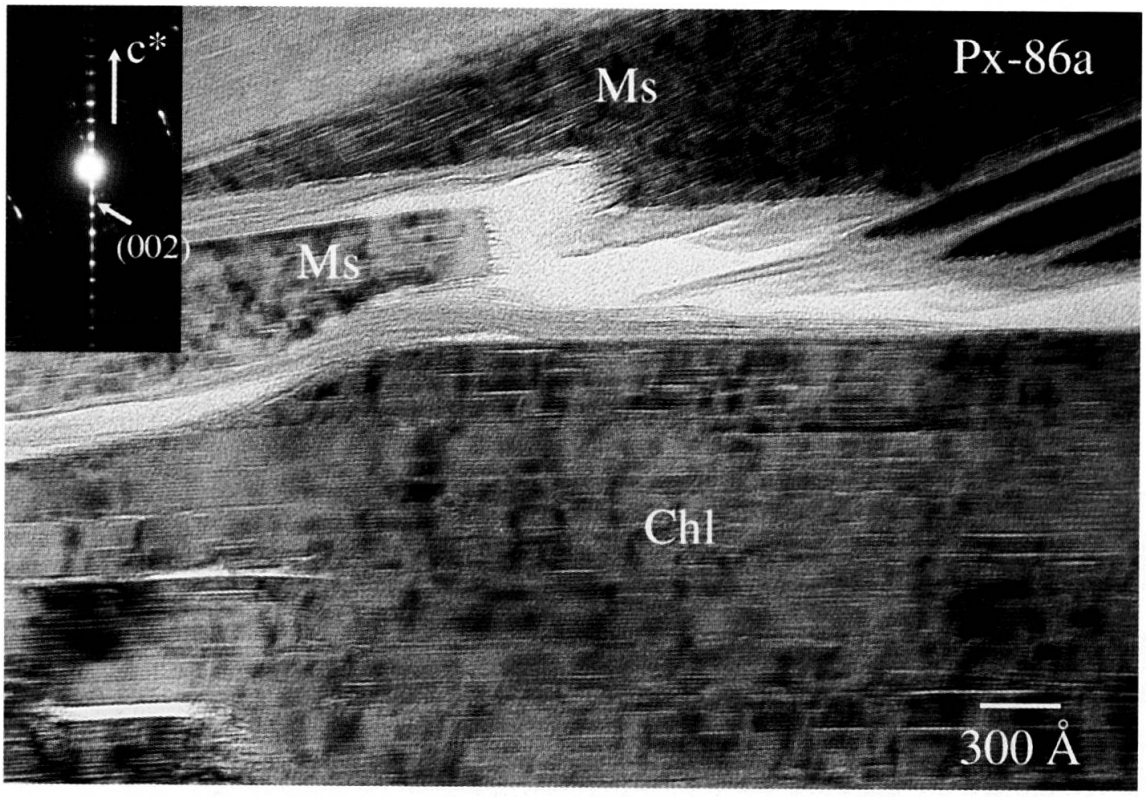

Fig. 9 A thick chlorite packet with defects that forms a low-angle boundary with thinner mica crystals. SAED shows slight streaking along the chlorite basal reflections.

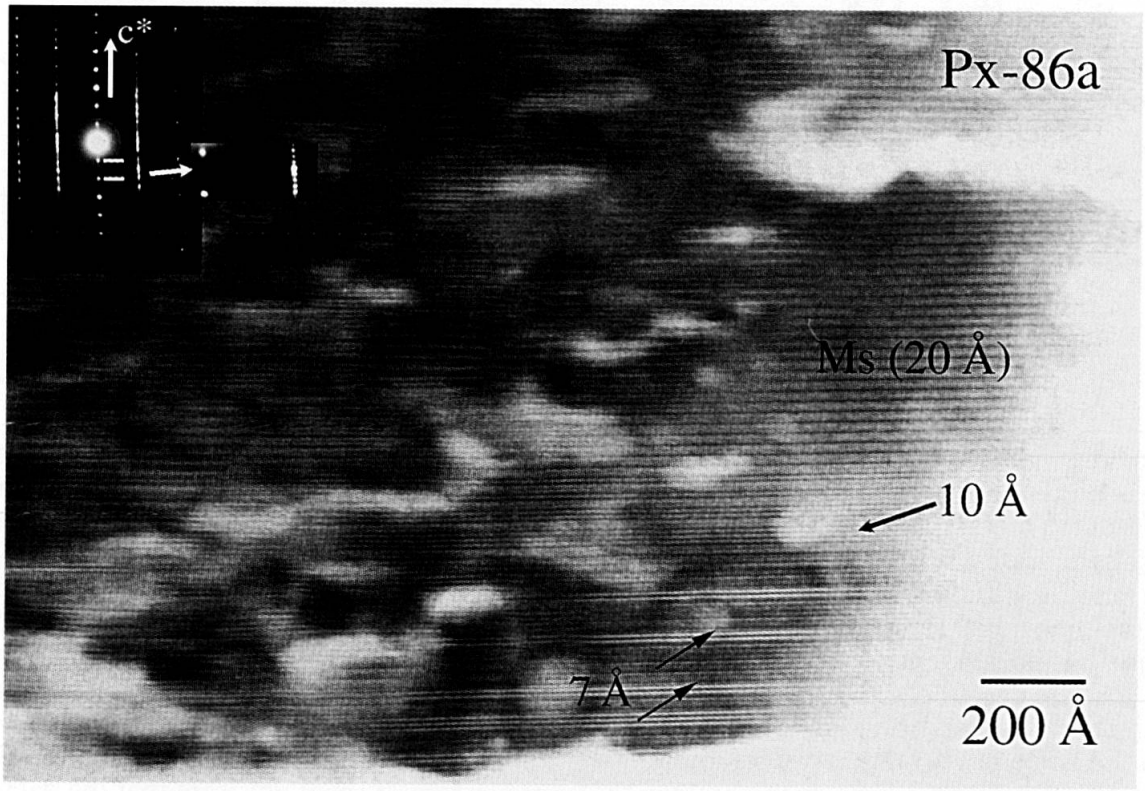

Fig. 10 Lattice-fringe image of muscovite crystal in which 7-Å layers occur randomly. SAED pattern (inset) shows a long period stacking sequence of 7 layers that has been enlarged.

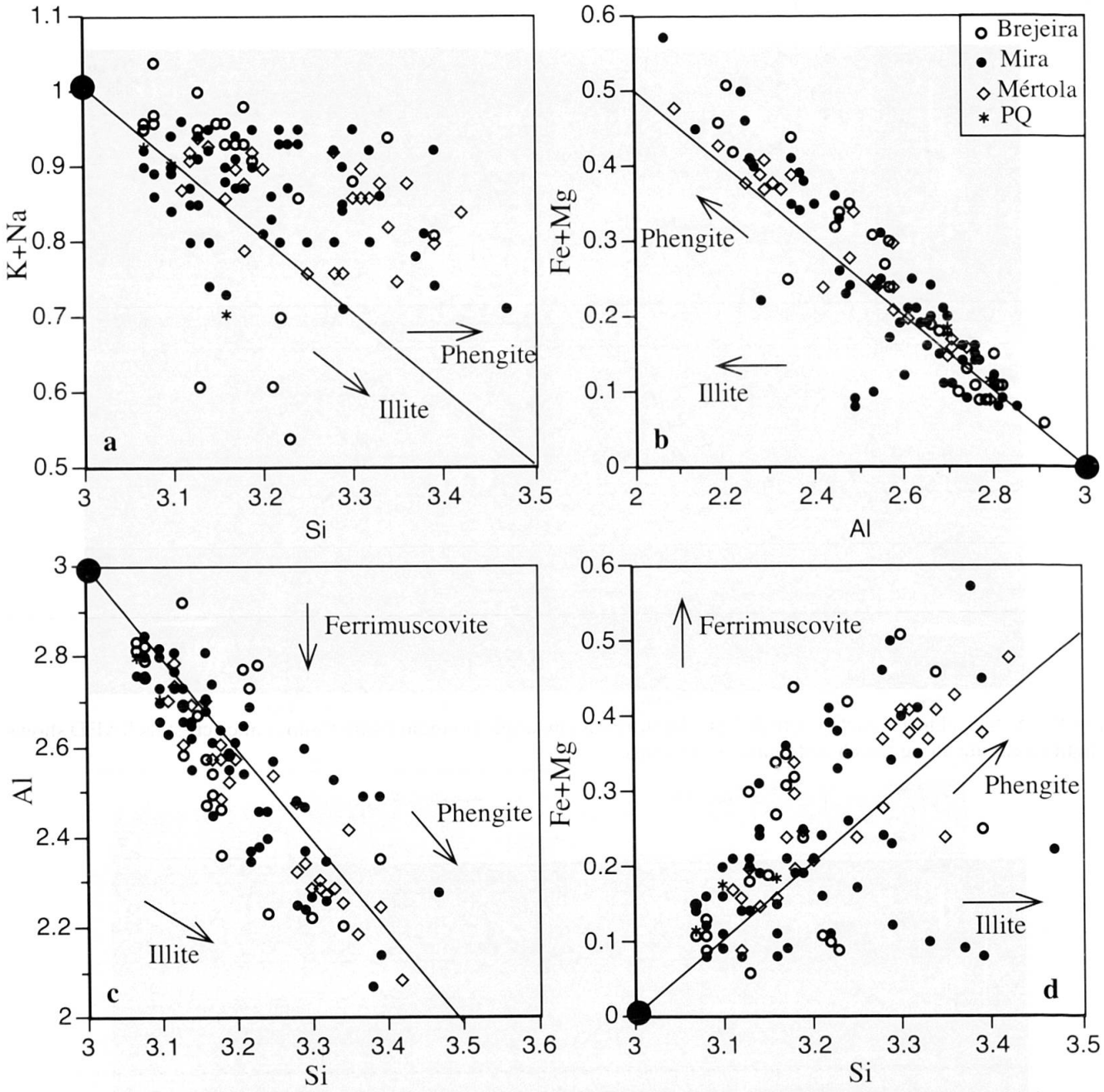

Fig. 11 Chemical composition diagrams of micas of the sandstones from the SPZ, black points and solid lines respectively indicate the theoretical muscovite position and corresponding exchange vectors.

4.5.1. Dioctahedral micas

The structural formulae of dioctahedral micas normalised to $O_{10}(OH)_2$ are presented in Table 3. The results indicate a lack of chemical homogeneity, not only in differences among samples, but also within individual samples (Fig. 11). Even so, there are certain tendencies throughout the sequence that are described below.

Illitic substitution is only somewhat more evident in the Brejeira Formation, where a few values of up to ≈0.6–0.7 a.f.u. have been obtained for the sum of interlayer cations, but the degree of substitution tends to decrease in micas of the stratigraphically lower formations (Fig. 11a). In addition, the Brejeira Formation also contains true muscovite with interlayer cation sums of 1 a.f.u. Excess of Si is caused by both illitic (Fig. 11a) and phengitic components (Figs. 11c–d). Despite the heterogeneity of the data, the ranges of variation of the chemical parameters not related to the magnitude of the phengitic component, Fe+Mg, Si $(Al^{VI}Al^{IV})_{-1}$, tend to decrease as the metamorphic grade increases, the correlations gradually fitting the phengitic theoretical trend better. The diagrams (Figs. 11b–c) illustrate that the data closest to the theoretical trends are those of the Mértola Formation, in which the Si-Al correlation is very

Table 3 Representative SEM data for micas[1] normalized to $O_{10}(OH)_2$.

Samples	Si	Al^{IV}	Al^{VI}	Fe	Mg	Ti	Σ oct.	K	Na	Σ inter.
Brejeira Formation										
Pc-11a/2	3.15	0.85	1.80	0.08	0.09	0.02	2.00	0.75	0.20	0.95
Pc-11a/9	3.24	0.76	1.46	0.22	0.19	0.14	2.01	0.85	0.00	0.85
Pf-23a/2	3.34	0.66	1.53	0.23	0.22	0.02	2.00	0.90	0.03	0.93
Pf-23a/3	3.13	0.87	1.70	0.13	0.16	0.03	2.02	0.91	0.08	0.99
Pf-23a/6*	3.08	0.92	1.82	0.06	0.06	0.05	2.00	0.89	0.06	0.95
Pf-23a/18*	3.13	0.87	2.04	0.02	0.02	0.01	2.10	0.48	0.12	0.60
Mira Formation										
Pi-33a/2*	3.14	0.86	1.70	0.21	0.11	0.01	2.02	0.81	0.13	0.94
Pi-33a/5*	3.29	0.71	1.66	0.12	0.22	0.03	2.03	0.85	0.00	0.85
Pi-33a/6*	3.13	0.87	1.79	0.08	0.11	0.03	2.01	0.82	0.12	0.94
Pi-33a/14	3.47	0.53	1.75	0.10	0.12	0.01	1.98	0.63	0.08	0.71
Pi-33a/17	3.13	0.87	1.86	0.11	0.03	0.01	2.01	0.68	0.23	0.91
Pj-39a/3*	3.08	0.92	1.88	0.07	0.04	0.03	2.03	0.76	0.10	0.86
Pj-39a/10	3.19	0.81	1.74	0.09	0.15	0.02	2.01	0.80	0.15	0.95
Pj-39a/13	3.33	0.67	1.86	0.05	0.05	0.00	1.96	0.66	0.20	0.86
Pk-42a/8*	3.22	0.78	1.59	0.23	0.17	0.03	2.01	0.77	0.18	0.95
Pk-42a/12*	3.07	0.93	1.83	0.09	0.04	0.05	2.01	0.82	0.08	0.90
Pk-42a/14	3.18	0.82	1.82	0.08	0.10	0.02	2.02	0.81	0.06	0.87
Pl-45a/3	3.07	0.93	1.83	0.07	0.08	0.04	2.02	0.87	0.05	0.92
Pl-45a/9	3.16	0.84	1.88	0.04	0.06	0.02	2.00	0.72	0.16	0.88
Pl-45a/10	3.37	0.63	1.87	0.04	0.05	0.01	1.97	0.71	0.07	0.78
Pm-50a/9	3.23	0.77	1.69	0.17	0.15	0.01	2.03	0.81	0.06	0.87
Pm-50a/10	3.10	0.90	1.92	0.07	0.02	0.01	2.03	0.69	0.16	0.85
Pn-53a/3	3.10	0.90	1.80	0.15	0.05	0.01	2.01	0.75	0.19	0.94
Pn-53a/5	3.17	0.83	1.91	0.04	0.06	0.01	2.01	0.77	0.10	0.87
Pn-53a/6	3.29	0.71	1.76	0.12	0.11	0.01	2.00	0.73	0.11	0.84
Po-57a/2	3.14	0.86	1.80	0.19	0.04	0.02	2.06	0.72	0.02	0.74
Po-57a/3*	3.12	0.88	1.89	0.09	0.05	0.01	2.04	0.62	0.18	0.80
Po-57a/7*	3.08	0.92	1.92	0.05	0.03	0.01	2.02	0.70	0.20	0.90
Mértola Formation										
Pp-64a/9	3.30	0.70	1.59	0.20	0.20	0.02	2.02	0.79	0.07	0.86
Pp-64a/16	3.39	0.61	1.64	0.13	0.25	0.01	2.03	0.76	0.04	0.80
Pq-67a/5	3.36	0.64	1.55	0.22	0.21	0.02	2.00	0.85	0.04	0.89
Pq-67a/12	3.14	0.86	1.85	0.05	0.10	0.01	2.01	0.83	0.09	0.92
Ps-73a/8	3.18	0.82	1.67	0.23	0.12	0.02	2.03	0.80	0.09	0.89
Ps-73a/11	3.33	0.67	1.62	0.15	0.22	0.02	2.01	0.84	0.04	0.88
Ps-73a/15	3.11	0.89	1.81	0.09	0.08	0.04	2.03	0.75	0.13	0.87
Pu-75a/15	3.42	0.58	1.52	0.19	0.29	0.02	2.02	0.83	0.01	0.84
Pu-75a/17	3.13	0.87	1.74	0.09	0.10	0.06	2.00	0.90	0.03	0.93
PQ Formation										
Px-86a/3*	3.16	0.84	1.86	0.10	0.08	0.04	2.07	0.62	0.08	0.70
Px-86a/5*	3.10	0.90	1.81	0.12	0.06	0.04	2.01	0.84	0.06	0.90
Px-86a/11	3.07	0.93	1.87	0.06	0.05	0.03	2.01	0.80	0.12	0.92

[1] * indicates mica stack analyses.

high, with a coefficient of correlation that reaches $r = -0.95$.

The sum of octahedral cations is in general only slightly higher than 2 a.f.u., which is proof of the quality of the analyses (Table 3). Mn and Ca, although quantified, are not included in the table of data as their amounts are <0.01 a.f.u. Ti, however, is always present and in significant amounts (0.01–0.05 a.f.u.) that occasionally reach values of >0.25 a.f.u. Na contents are higher (Na/(Na+K)= 0.10, σ= 0.06), in some micas even surpassing K (Na/(Na+K)= 0.42–0.65 a.f.u.). Table 4 presents the data corresponding to intermediate Na-K mica, both samples are from the Mira Formation. They correspond to mica-chlorite stacks, with micas with different proportions of Na/K co-existing and producing different intensities of the grey scale in the BSE images (Fig. 2b). These Na-rich micas have also been found in the rock matrix by HRTEM/AEM, for example the Fig. 5, corresponding to the Pk-42a sample, shows a Na-K mica (K= 0.36, a.f.u. and Na= 0.36 a.f.u.) that con-

Table 4 Representative chemical compositions for intermediate Na-K micas normalized to $O_{10}(OH)_2$.

Samples	Si	Al^{IV}	Al^{VI}	Fe	Mg	Ti	Σ oct.	K	Na	Na/Na+K
Pi-33a/10	3.30	0.70	1.79	0.17	0.11	0.01	2.08	0.39	0.35	0.47
Pi-33a/11	3.14	0.86	1.92	0.03	0.04	0.01	2.01	0.52	0.37	0.42
Pn-53a/11	3.08	0.92	1.97	0.01	0.03	0.01	2.02	0.26	0.65	0.71
Pn-53a/12	3.12	0.88	1.95	0.02	0.05	0.01	2.03	0.30	0.55	0.65

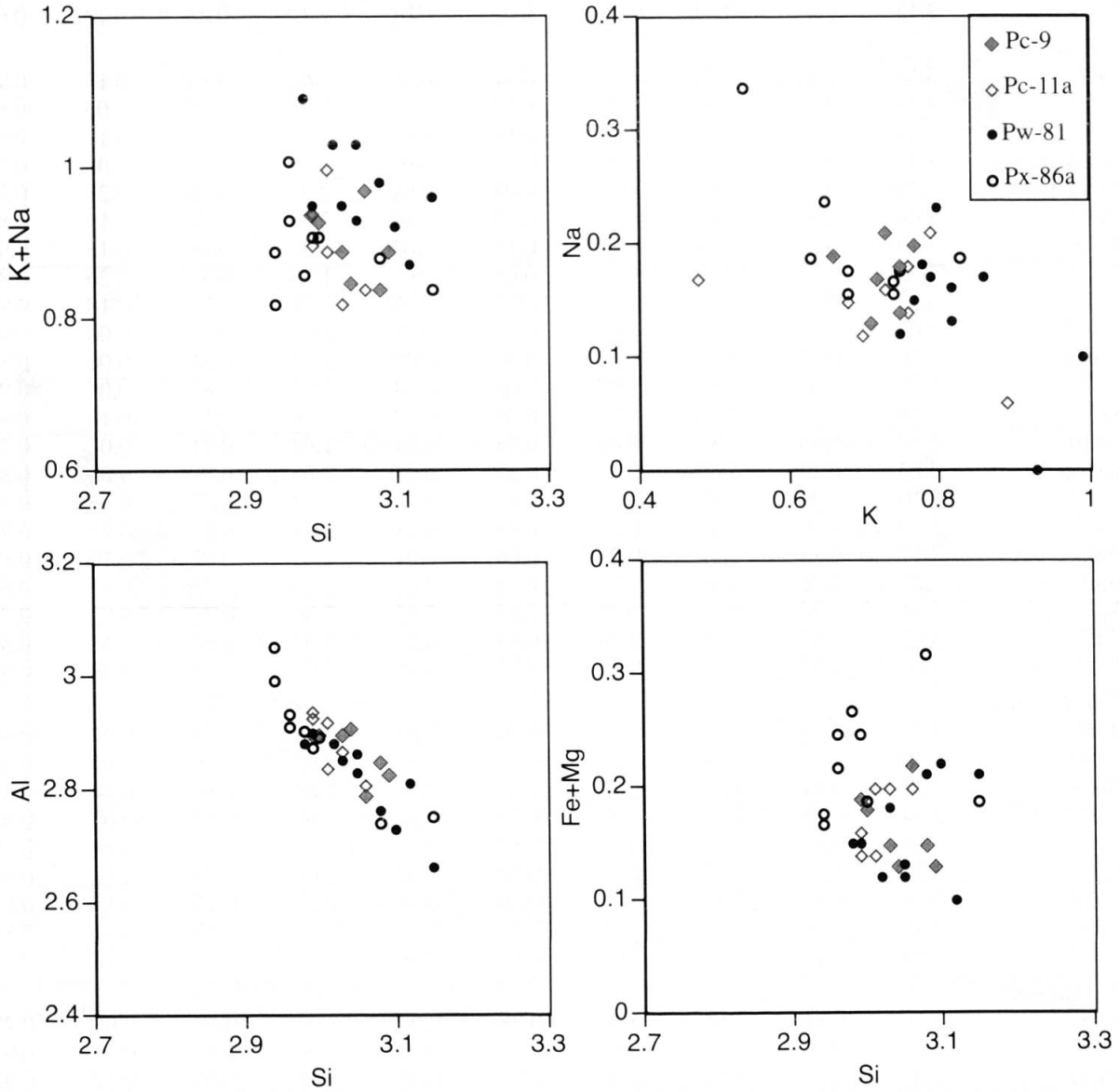

Fig. 12 Diagrams of the chemical composition of micas of metapelites and equivalent sandstones from SPZ based on AEM analysis. Solid symbols—pelites, open symbols—corresponding sandstones.

firms the presence of these intermediate micas already established by XRD.

BSE images in Z-contrast mode have been used to select analysis points in crystals with an apparent thickness of <10 μm and in the stacks. In some cases, several analyses have been performed along stacks and in crystals along different orientations. It has been noted that the stacks, in contrast to other cases (Dalla Torre et al., 1996), lack compositional zoning and no systematic compositional differences can be detected between them and analyses corresponding to matrix micas, except more homogeneous and lower phengite components in the intergrowths (see Table 3, analyses marked by an asterisk).

When comparing K-dioctahedral mica analyses of coeval sandstones and metapelites, some minor chemical differences observed might be

Table 5 Representative chemical compositions for chlorites normalized to $O_{10}(OH)_8$.

Samples	Si	Al^{IV}	Al^{VI}	Fe	Mg	Mn	Ti	Σ oct.	Fe/Fe+Mg
Mira Formation									
Pj-39a/1	2.62	1.38	1.52	2.53	1.85	0.03	0.00	5.93	0.58
Pj-39a/5	2.67	1.33	1.60	2.47	1.79	0.02	0.00	5.87	0.58
Pj-39a/8	2.63	1.37	1.48	2.62	1.82	0.03	0.01	5.96	0.59
Pj-39a/11	2.78	1.22	1.20	1.89	2.93	0.02	0.00	6.04	0.39
Pk-42a/1	2.75	1.25	1.71	2.59	1.46	0.04	0.00	5.79	0.64
Pk-42a/4	2.66	1.34	1.62	2.76	1.46	0.03	0.00	5.86	0.65
Pk-42a/6	2.80	1.20	1.60	2.78	1.39	0.04	0.00	5.80	0.67
Pk-42a/9	2.67	1.33	1.67	2.61	1.52	0.03	0.00	5.83	0.63
Pk-42a/15	3.05	0.95	1.40	2.43	1.94	0.03	0.00	5.81	0.56
Pl-45a/1	2.81	1.19	1.68	2.55	1.51	0.04	0.00	5.77	0.63
Pl-45a/4	2.81	1.19	1.67	2.48	1.58	0.03	0.00	5.77	0.61
Pm-50a/2	2.66	1.34	1.67	2.64	1.50	0.04	0.01	5.86	0.64
Pm-50a/5	2.70	1.30	1.67	2.70	1.42	0.05	0.01	5.85	0.66
Pm-50a/8	2.74	1.26	1.62	2.85	1.37	0.04	0.01	5.89	0.68
Po-57a/8	2.62	1.38	1.54	2.85	1.52	0.04	0.00	5.95	0.65
Mértola Formation									
Pp-64a/2	2.67	1.33	1.52	2.60	1.76	0.04	0.00	5.91	0.60
Pp-64a/4	2.72	1.28	1.60	2.41	1.81	0.04	0.00	5.85	0.57
Pp-64a/5	2.77	1.23	1.60	2.55	1.65	0.03	0.00	5.83	0.61
Pq-67a/3	2.62	1.38	1.45	2.82	1.74	0.03	0.00	6.04	0.62
Pq67-a/4	2.89	1.11	1.36	2.70	1.77	0.04	0.00	5.88	0.60
Pq67-a/14	2.77	1.23	1.48	2.79	1.60	0.03	0.00	5.91	0.64
Ps-73a/1	3.09	0.91	0.94	2.61	1.89	0.02	0.27	5.73	0.58
Ps-73a/3	3.11	0.89	1.24	2.40	2.23	0.02	0.00	5.91	0.52
Ps-73a/4	3.06	0.94	1.57	2.36	1.77	0.03	0.00	5.73	0.57
Ps-73a/6	2.91	1.09	1.07	2.97	1.67	0.02	0.16	5.89	0.64
Ps-73a/7	3.02	0.98	1.00	2.81	1.74	0.03	0.22	5.79	0.62
Ps-73a/13	3.14	0.86	1.36	2.42	2.02	0.02	0.00	5.83	0.54
Ps-73a/16	2.66	1.34	1.51	2.91	1.47	0.05	0.00	5.94	0.66
Pu-75a/1	2.92	1.08	1.42	2.91	1.45	0.04	0.01	5.83	0.67
Pu-75a/9	2.81	1.19	1.59	2.77	1.40	0.05	0.00	5.80	0.66
Pu-75a/13	2.74	1.26	1.54	2.85	1.50	0.04	0.01	5.94	0.66
Pu-75a/16	2.83	1.17	1.59	2.81	1.35	0.05	0.00	5.80	0.68
PQ Formation									
Px-86a/4	2.62	1.38	1.59	3.09	1.18	0.03	0.00	5.90	0.72
Px-86a/8	2.73	1.27	1.82	2.66	1.24	0.00	0.00	5.72	0.68

due to instrumental factors, because the sandstone phyllosilicates could be analysed by SEM due to their larger grain size, whereas those in the metapelites could only be analysed by AEM (ABAD et al., 2001). Therefore, in order to eliminate instrument-derived differences, we prepared grids from samples Pc-11a and Px-86a, which are sandstones located very close to shale samples Pc-9 and Px-81, respectively. Figure 12 shows for different samples a mica population with no significant chemical differences related to lithology. Thus, when the data of analyses performed under similar conditions are compared, they verify that the shales and the sandstones have very similar mica populations. Other research studies have found that AEM may underestimate Si (ABAD et al., 2002, LÓPEZ-MUNGUIRA et al., 2002), which is most likely why, based on the SEM data, the sandstones micas appear to be slightly more phengitic.

4.5.2. Chlorite

Table 5 presents the chemical data for chlorite, which is trioctahedral and Fe-rich, corresponding to the species chamosite. The Mira Formation is characterised by chlorite that has less Si and more Al and that is homogeneous, whereas the Mértola Formation has a very heterogeneous chlorite population, ranging widely in Si (2.6–3.1) a.f.u. and Al (2–2.9) a.f.u (Fig. 13). A few Ti analyses reveal values of > 0.20 a.f.u., corresponding to chlorite in stacks which have the optical appearance of biotite (Fig. 2f). Small amounts of K, Na and Ca have been found, thought to be a result of con-

tamination by white mica in the fine intergrowths (<5 μm) of the phyllosilicates in these rocks. Therefore, the chlorite formulae have been recalculated (see techniques section).

The ratio of Fe/(Fe+Mg), with a range of 0.39–0.72, shows no clear trends in the sequence and we have detected no increase in Mg, with increase in grade as has been found in other prograde sequences (BEVINS et al., 1991). The ratios are within the range of values characteristic of diagenetic chlorites in metamorphic rocks (LI et al., 1994b).

5. Discussion

The mineral processes occurring during very low-grade metamorphism imply a general lack of textural and chemical equilibrium. This heterogeneity, with increasing metamorphic grade and the development of slaty cleavage, is progressively reduced, and the texture and composition of minerals converge towards a stable state.

Optical microscopy, SEM (Fig. 2) and low-magnification TEM (Fig. 8a) studies reveal evident petrographic differences between the coeval sandstones and metapelites of the SPZ, such as the greater degree of cleavage in finer-grained rocks due to the deformation (see Fig. 4 in ABAD et al., 2001 vs. Fig. 2, this work) or the common presence of stacks in the sandstones samples which must represent microstructural sites that can provide elements for the transformations and the growth of new minerals during cleavage formation and fluid circulation (BEACH, 1979). However, the differences are minimal when comparing such features as mineralogy, crystal-chemical parameters, chemical analyses of the phyllosilicates and the TEM lattice-fringe images. In fact, the sandstone matrix is very similar to that of the interbedded pelite units.

According to BOLES and FRANKS (1979), most of the water that moves through the interbedded sandstones is derived from migration of original shale pore water and from clay dehydration reactions in shales; however, other studies have found that shales appear to act as a closed system during diagenesis (BLOCH and HUTCHEON, 1992; LYNCH and LAND, 1996). Therefore, there are ambiguous results about the relationship between diagenesis in adjacent sandstones and shales. Diagenesis consists of physical effects such as compaction, dissolution of some minerals which are out of equilibrium, and the precipitation of more stable minerals which progressively reduce porosity and permeability during burial. The chemical processes become more difficult during deeper burial between 70–140 °C, because the slow flow rates make it difficult to transport chemically reactive fluids more than a few meters (THYNE, 2001; SURDAM et al., 1989). The abundant studies on diagenetic coeval shales and sandstones seem to suggest that when the late diagenesis-low anchizone is reached both lithologies act as a closed system to mass-transfer (HASZELDINE et al., 2000). In such conditions, the phyllosilicate-rich matrix of the greywackes would play a very similar role to that of shales, with the only significant difference being in the relative proportions of matrix/detrital grains. This difference would be very significant in macroscopic and mechanical aspects or in the Si/Al ratio, but not at the nano-scale nor in the chemistry of layer silicates. Homogenisation is strongly controlled by the factor time. According to FERREIRO MÄHLMANN (2001) the duration of peak-temperature metamorphism plays an important role in the attainment of the equilibri-

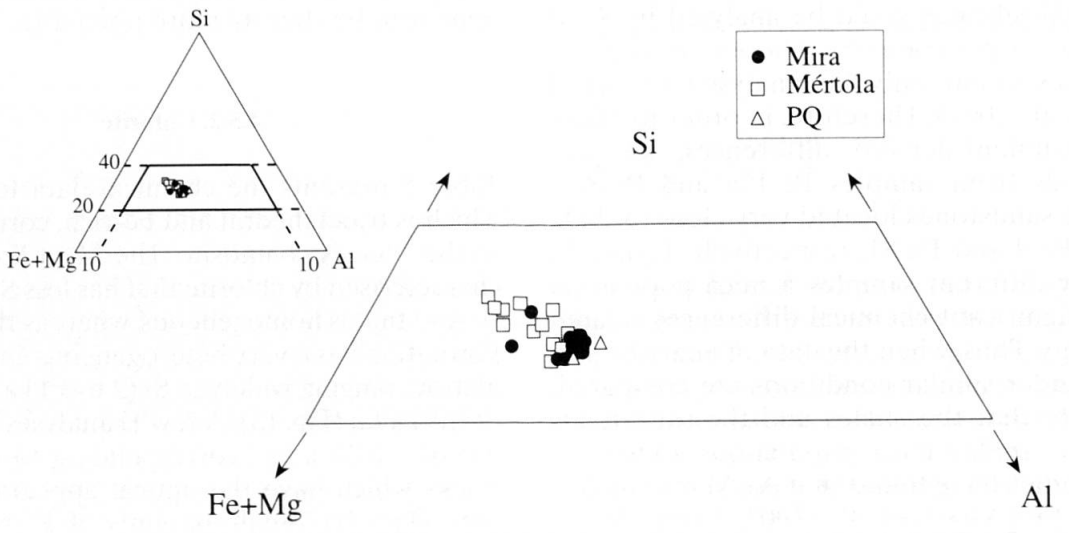

Fig. 13 Compositional diagram of chlorites.

um among different metamorphic-grade parameters.

5.1. MINERALOGY, CRYSTAL-CHEMICAL PARAMETERS, TEXTURE AND POLYTYPES OF PHYLLOSILICATES

The mineral assemblages of the sandstones established by XRD are similar to those of the metapelites. The main difference is that the latter have a higher proportion of phyllosilicates. Albite, identified only in the more metamorphosed metapelitic rocks, is a common phase in the sandstones, at times co-existing with K-feldspar independently of the presence of Na-K micas. The angular shape and large size of grains suggest a detrital origin. The presence of K-feldspar, kaolinite and illite is common in sandstones and the formation of illite has been usually attributed to the dissolution of K-feldspar, which serves as a potassium source and converts the kaolinite into illite (BJØRLYKKE and AAGAARD, 1992; HASSOUTA et al., 1999; LE GALLO et al., 1998).

The IC values are similar for both sandstones and shales; i.e., they are not related to the grain sizes of the samples (Fig. 3). This agrees with the crystallite-size measurements for lattice-fringe images (see TEM observations section) which revealed a range of sizes of mica packets in sandstones very similar to those previously quantified in the equivalent metapelites (ABAD et al., 2001). In both the sandstones and the shales, the differences in IC values between the two size fractions (bulk and < 2 μm) in the Brejeira and Mira Formations indicate detrital and authigenic mica populations that are not in equilibrium. In contrast, in the Mértola Formation the IC values show much less variation, suggesting a closer approach towards metamorphic equilibration of the micas.

The ranges found for the d_{001} and the *b* parameters of white mica in sandstones also coincide with those for the shales (ABAD et al., 2001). This is a logical consequence of the lack of significant chemical differences between the micas of both kinds of rocks (Fig. 12).

TEM data reveal characteristics at the nanoscale (high-contrast fringes, strain fields, and layer terminations) induced by deformation, that indicate the development of a tectonic fabric in low-grade metamorphic terranes, in agreement with the observations of the associated metapelites. Nonetheless, these features are not observable by SEM, where the appearance of all the sandstones is very similar, in contrast with metapelites, where the presence of a tectonic fabric is evident in the highest-grade samples (ABAD et al., 2001).

The Na-K micas present in the matrix of the sandstones of this study display the same chemical and textural characteristics as described for the corresponding metapelites (see ABAD et al., 2001, Fig. 5 vs. Fig. 5 herein).

In addition to the 2M polytype, long-period stacking sequences of 7 layers are present in white micas (Fig. 10, inset), which may be related to the combination of simple polytypes. LÓPEZ-MUNGUIRA and NIETO (2000) reported long-period stacking sequences of 4, 5 and 6 layers in K-rich micas in a low-grade metamorphic sequence from the Ossa-Morena Zone (SW Spain). In both cases, the samples are coarser than metapelites. These complex stacking sequences have also been found recently by DO CAMPO and NIETO (submitted) in very low-grade pelitic samples of the Puncoviscana Formation (NW Argentina). There is no clear idea concerning the genetic meaning of the high-order polytypes, but it is inferred that the co-existence of different polytypes indicates a lack of equilibrium and that the presence of one or the other must be determined by local conditions.

5.2. CHEMICAL COMPOSITIONS OF ROCKS AND PHYLLOSILICATES

As expected, the whole-rock analyses of major elements of the sandstones are richer in Si than those of the coeval metapelites. Nevertheless, the relative proportions of other elements are very similar, except for lower K contents and the slightly higher Na contents in sandstones than in shales. HASZELDINE et al. (2000) support that geochemical data sets from shales and enclosed sandstones from the USA Gulf Coast show Al and K loss from sands that are probably transferred into the enclosing muds. Mass balance calculations indicate that burial diagenesis of shales is an open-system process that requires addition of K_2O and Al_2O_3 and results in loss of SiO_2 that would be the source of quartz-overgrowth cements in the associated sandstones (LYNCH et al., 1997).

One of the advantages of sandstones minerals in relation to those in shales is that they can be analysed by SEM or electron microprobe with comparatively little contamination problems. ABAD et al. (2002) have demonstrated that EDX analyses of phyllosilicates performed in the SEM are able to produce results very similar in quality to those of EMPA; thus, the results presented in Tables 3–5 have allowed us to characterise the mineral composition of the SPZ more accurately than the AEM shale data obtained by ABAD et al. (2001).

The scattering of mica compositions is principally produced by several singular chemical

changes along the phengitic vector (Figs. 11b, c and d) with minor chemical differences along the illitic vector (Fig. 11a). The same tendencies have been described for the pelitic rocks of the Variscan Belt foreland in the Narcea Antiform (ABAD et al., 2002). On the other hand, in the SPZ the effect of the ferriceladonite component is minor due to the low overall quantity of Fe in these micas. Only a slight progression towards equilibrium is shown by a better chemical evolution progress along the theoretical phengitic vector of the mica composition of the Mértola Formation, which has the highest metamorphic-grade.

As in metapelites (ABAD et al., 2001) chlorite is absent in samples with low Fe and Mg contents, as for instance, in the Brejeira Formation (see Table 2). However, in contrast to the metapelites, where the chlorite is rich in Si and also Fe, the sandstones show a greater proportion of chlorite with less Si and a higher Fe content.

5.3. ORIGIN OF PHYLLOSILICATE STACKS

The origin of chlorite-mica stacks has been much discussed in recent years. According to MILODOWSKI and ZALASIEWICZ (1991), stack distribution is strongly related to the sedimentology, being most abundant in the coarser-grained fraction, at the base of Bouma turbidite units. LI et al. (1994b) distinguished different modes of occurrence of white mica and chlorite in slates from Central Wales (U.K.) and reported differing compositions in stacks versus those of the matrix suggesting that, to some extent, the larger packet size of the stacks may have been inherited from a phyllosilicate precursor. The compositional differences between the matrix and the phyllosilicate precursor reflect several limits to diffusion such as diffusion distances and, hence, the size of "equilibration" domains controlled by the low temperature of late diagenesis and low-grade metamorphism. In terms of textures and composition white micas in the stacks described here, are generally similar to those reported for micas in stacks of other Palaeozoic turbidites (DIMBERLINE, 1986; MILODOWSKI and ZALASIEWICZ, 1991; LI et al. 1994b).

The direct alteration of biotite to chlorite during diagenesis and low-grade metamorphism has been described by a number of workers (VEBLEN and FERRY, 1983; MORAD, 1990; MORAD and ALDAHAN, 1986; JIANG and PEACOR, 1994; LI et al. 1994b). Textural and chemical data for the chlorite-mica stacks of the SPZ sandstones suggest a detrital precursor because of their size and the presence of crenulation cleavage in most of them attributable to prior deformational stages. Moreover, the high Ti contents in chlorites belonging to the stacks suggest the possibility of alteration of detrital biotite to chlorite. The packets of white mica within chlorite in stacks appear to fill cleavage openings in the chlorite, as observed in BSE images (Figs. 2c, d and f).

Although the stacks appear to be detrital in origin, the chlorite-mica-kaolinite association, and specially the presence of Na-K mica, are consistent with modification by metamorphic processes. Moreover, no significant differences have been detected at nano-scale between stack-forming phyllosilicates and those of matrix.

5.4. CONCLUDING REMARKS

In very low-grade metamorphic turbidite sequences, the grain size of the rock should not be a limiting criterion in the sampling, particularly if very fine-grained rocks are scarce or commonly affected by weathering since, after diagenetic processes, both metapelites and greywackes provide similar data. Illite crystallinity and traditional crystal-chemical parameters, such as d_{001} and b, produce equivalent and inter-changeable relations for phyllosilicates of the sandstones and shales and no differences have been found between the phyllosilicates in the lattice-fringe images, polytypes, chemical compositions or crystalline-domain size of the two types of rocks. That is to say, sandstones and samples with intermediate characteristics between sandstones and shales may provide valid results and, in any case, SEM analysis produces more accurate results in larger-grained rocks than in typical metapelites. In contrast, one of the main limitations of studying sandstones with the classic XRD method used for pelitic rocks is the relatively small phyllosilicates/quartz ratio which makes it difficult to determine some crystal-chemical parameters.

Acknowledgments

We thank M.M. Abad Ortega and I. Guerra from the Scientific Instrument Center of the University of Granada for their help with HRTEM and SEM work respectively. We are also grateful to Christine Laurin for revising the English text. Thanks are extended to R.J. Merriman, D.R. Peacor and L. Warr for their critical reviews and very helpful comments and suggestions. Financial support was supplied by Research Project nº BT 2000-0582 and FPI research grant to I.A., both of the Spanish Ministry of Science and Technology and Research Group RNM-0179 of the Junta de Andalucía.

References

ABAD, I., MATA, M.P., NIETO, F. and VELILLA, N. (2001): The phyllosilicates in diagenetic-metamorphic rocks of the South Portuguese zone, southwestern Portugal .Can. Mineral. 39, 1571–1589.

ABAD, I., NIETO, F. and GUTIÉRREZ-ALONSO (2002): Textural and chemical changes in slate-forming phyllosilicates of the foreland-hinterland transition in the low-grade metamorphic belt of the NW Iberian Variscan Chain. Schweiz. Mineral. Petrogr. Mitt. (submitted).

AHN, J.H. and PEACOR, D.R. (1986): Transmission and analytical electron microscopy of the smectite-to-illite transition. Clays Clay Mineral. 34, 165–179.

ÁRKAI, P., MATA, M.P., GIORGETTI, G., PEACOR, D.R. and TÓTH, M. (2000): Comparison of diagenetic and low-grade metamorphic evolution of chlorite in associated metapelites and metabasites: an integrated TEM and XRD study. J. Metamorphic Geol. 18, 531–550.

BEACH, A. (1979): Pressure solution as a metamorphic process in deformed terrigenous sedimentary rocks. Lithos 12, 51–58.

BEVINS, R.E., ROBINSON, D. and ROWBOTHAM, G. (1991): Compositional variations in mafic phyllosilicates from regional low-grade metabasites and application of the chlorite geothermometer. J. Metamorphic Geol. 9, 711–721.

BJØRLYKKE, K. and AAGAARD, P. (1992): Clay minerals in North Sea sandstones. In: HOUSEKNECHT, D.W. and PITMAN, E.D. (eds): Origin, diagenesis, and petrophysics of clay minerals in sandstones SEPM Special Publication. 47, 65–80.

BLOCH, J. and HUTCHEON, I.E. (1992): Shale diagenesis: A case study from the Albian Harmon Member (Peace River Formation), Western Canada. Clays Clay Mineral. 40, 682–699.

BOLES, J.R. and FRANKS, S.G. (1979): Clay diagenesis in Wilcox sandstones of southwest Texas: Implications of smectite diagenesis on sandstone cementation. J. Sedimentary Geol. 49, 55–69.

CLIFF, G. and LORIMER, G.W. (1975): The quantitative analysis of thin specimens. J. Microscopy 103, 203–207.

COOPER, A.H. and MOLINEUX, S.G. (1990): The age and correlation of the Skiddaw Group (early Ordovician) sediments in the Cross Fell inlier (northern England). Geol. Mag. 127, 147–157.

DALLA TORRE, M., LIVI, J.T.K., VEBLEN, D.R. and FREY, M. (1996): White K-mica evolution from phengite to muscovite in shales and shale matrix melange, Diablo Range, California. Contrib. Mineral. Petrol. 123, 390–405.

DIMBERLINE, A.J. (1986): Electron microscope and microprobe analysis of chlorite-mica stacks in the Wenlock turbidites, mid Wales, U.K. Geol. Mag. 123, 299–306.

DO CAMPO, M. and NIETO, F. (submitted): Transmission electron microscopy study of very low-grade metamorphic evolution in Neoproterozoic pelites of the Puncoviscana Formation (Cordillera Oriental, NW Argentina)

FERREIRO MÄHLMANN, R. (2001): Correlation of very low grade data to calibrate a thermal maturity model in a nappe tectonic setting, a case study from the Alps. Tectonophysics 334, 1–33.

FOLK R.L. (1968): Petrology of sedimentary rocks. Hampills, Austin Texas. 170 pp.

GLASMANN, J.R., LUNDEGARD, P.D., CLARK, R.A., PENNY, B.K. and COLLINS, I.D. (1989): Geochemical evidence for the history of diagenesis and fluid migration; Brent sandstone, Heather Field, North Sea. Clay Mineral. 24, 255–284.

GIORGETTI, G., MEMMI, I. and NIETO F. (1997): Microstructures of intergrown phyllosilicate grains from Verrucano metasediments (northern Apennines, Italy). Contrib. Mineral. Petrol. 128, 127–138.

GUIDOTTI, C.V., YATES, M.G., DYAR, M.D. and TAYLOR, M.E. (1994): Petrogenetic implications of the Fe^{3+} content of muscovite in pelitic schists. Am. Mineral. 79, 793–795.

HASSOUTA, L., BUATIER, M.D., POTDEVIN, J.L. and LIEWIG, N. (1999): Clay diagenesis in the sandstones reservoir of the Ellon Field (Alwyn, North Sea). Clays Clay Mineral. 47, 269–285.

HASZELDINE, R.S., BRINT, J.F., FALLICK, A.E., HAMILTON, P.J. and BROWN, S. (1992): Open and restricted hydrologies. In: MORTON A.C., HASZELDINE R.S., GILES F.R. and BROWN S. (eds): Geology of the Brent Group. Geological Society (London) Special Publication 61, 401–419.

HASZELDINE, R.S., MACAULAY, A., MARCHAND, A., WILKINSON, M., GRAHAM, C.M., CAVANAGH, A., FALLICK, A.E. and COUPLES, G.D. (2000): Sandstone cementation and fluids in hydrocarbon basins. J. Geochem. Explor. 69–70, 195–200.

JIANG W.T. and PEACOR D.R. (1994): Formation of corrensite, chlorite and chlorite-mica stacks by replacement of detrital biotite in low-grade pelitic rocks. J. Metamorphic Geol. 12, 867–884.

KANTOROWICZ, J. (1984): The nature, origin and distribution of authigenic clay minerals from Middle Jurassic Ravenscar and Brent Group sandstones. Clay Mineral. 19, 359–375.

KEMP, A.E.S., OLIVER, G.J.H. and BALDWIN, J.R. (1985): Low-grade metamorphism and accretion tectonics: Southern Uplands terrain, Scotland. Mineral. Mag. 49, 335–344.

KISCH, H.J. (1991): Illite crystallinity: recommendations on sample preparation, X-ray diffraction settings, and interlaboratory samples. J. Metamorphic Geol. 9, 665–670

KRETZ, R. (1983): Symbols for rock-forming minerals. Am. Mineral. 68, 277–279.

LE GALLO, Y., BILDSTEIN, O. and BROSSE, E. (1998): Coupled reaction-flow modeling of diagenetic changes in reservoir permeability, porosity and mineral compositions. J. of Hydrology 209, 366–388.

LEISTEL, J.M., MARCOUX E., THIEBLEMONT, D., QUESADA C., SANCHEZ, A., ALMODOVAR, G.R., PASCUAL, E. and SAEZ R. (1998): The volcanic-hosted massive deposits of the Iberian Pyrite Belt. Mineralium Deposita 33, 2–30.

LI, G., PEACOR, D.R., MERRIMAN, R.J. and ROBERTS, B. (1994a): The diagenetic to low grade metamorphic evolution of matrix white mica in the system muscovite-paragonite in a mudrock from Central Wales, UK. Clays Clay Mineral. 42, 369–381.

LI, G., PEACOR, D.R., MERRIMAN, R.J., ROBERTS, B. and VAN DER PLUIJM, B.A. (1994b): TEM and AEM constraints on the origin and significance of chlorite-mica stacks in slates: an example from Central Wales, U.K. J. Struct. Geol. 16, 1139–1157.

LIVI, K.J.T., VEBLEN, D.R., FERRY, J.M. and FREY, M. (1997): Evolution of 2:1 layered silicates in low-grade metamorphosed Liassic shales of Central Switzerland. J. Metamorphic Geol. 15, 323–344.

LÓPEZ-MUNGUIRA, A., NIETO, F. (2000): Transmission electron microscopy study of very low-grade metamorphic rocks in Cambrian sandstones and shales, Ossa-Morena Zone, Southwest Spain. Clays Clay Mineral. 48, 213–223.

López-Munguira, A., Nieto, F. and Morata, D. (2002): Chlorite composition and geothermometry: A comparative HRTEM/AEM-EMPA-XRD study of Cambrian basic lavas from the Ossa Morena Zone, SW Spain. Clay Mineral. 37, 267–281.

Lynch, F.L. and Land, L.S. (1996): Diagenesis of calcite cement in Frio sandstones and its relationship to formation water chemistry. J. Sedim. Research. 66, 439–466.

Lynch, F.L., Mack, L.E. and Land, L.S. (1997): Burial diagenesis of illite/smectite in shales and the origins of authigenic quartz and secondary porosity in sandstones. Geochim. Cosmochim. Acta. 61, 1995–2006.

Masuda, H., Peacor, D.R. and Dong, H. (2001): Transmission electron microscopy study of conversion of smectite to illite in mudstones of tne Nankai through: Contrast with coeval metapelites. Clays Clay Mineral. 49, 109–118.

Mata, M.P., Giorgetti, G., Árkai, P. and Peacor, R.D. (2001): Comparison of evolution of trioctahedral chlorite/berthierine/smectite in coeval metabasites and metapelites from diagenetic to epizonal grades. Clays Clay Mineral. 49, 318–332.

Merriman, R.J. and Peacor, D.R. (1999): Very low-grade metapelites: mineralogy, microfabrics and measuring reaction progress. In: Frey, M. and Robinson, D. (eds): Low Grade-Metamorphism, 10–60. Blackwell Science, Oxford.

Milodowski, A.E. and Zalasiewicz, J.A. (1991): The origin and sedimentary, diagenetic and metamorphic evolution of chlorite-mica stacks in Llandovery sediments of central Wales, U.K. Geol. Mag. 128, 263–278.

Morad, S. (1990): Mica alteration reactions in Jurassic reservoir sandstones from the Haltenbanken area, offshore Norway. Clays Clay Mineral. 38, 584–590.

Morad, S. and Aldahan, A.A. (1986): Diagentic alteration of detrital biotite in Proterozoic sedimentary rocks from Sweden. Sedimentary Geol. 47, 95–107.

Munhá, J. (1983a): Hercynian magmatism in the Iberian Pyrite Belt. Mem. Serv. Geol. Portugal 29, 39–81.

Munhá, J. (1983b): Low-grade regional metamorphism in the Iberian Pyrite Belt. Comun. Serv. Geol. Portugal. 69, 3–35.

Munhá, J. (1990): Metamorphic evolution of the South Portuguese/Pulo do Lobo zone. In: Dallmeyer, R.D. and Martínez García E. (eds): Pre-Mesozoic Geology of Iberia, 363–368. Springer, Berlin.

Munhá, J. and Kerrich, R. (1980): Sea water-basalt interaction in spilites of the Iberian Pyrite Belt. Contrib. Mineral. Petrol. 73, 191–200.

Munhá, J., Oliveira, J.T., Ribeiro, A., Oliveira, V., Quesada, C. and Kerrich, R. (1986): Beja-Acebuches Ophiolite: characterization and geodynamic significance. Bol. Soc. Geol. Portugal 2, 13–31.

Nieto, F. (1997): Chemical composition of metapelitic chlorites: X-ray diffraction and optical property approach. Eur. J. Mineral. 9, 829–841.

Nieto, F., Ortega-Huertas, M., Peacor, D.R. and Aróstegui, J. (1996): Evolution of illite/smectite from early diagenesis through incipient metamorphism in sediments of the Basque-Cantabrian Basin. Clays Clay Mineral. 44, 304–323.

Nieto, F. and Sánchez-Navas, A. (1994): A comparative XRD and TEM study of the physical meaning of the white mica "crystallinity" index. Eur. J. Mineral. 6, 611–621.

Oliveira, J.T. (1990): South Portuguese Zone: Stratigraphy and synsedimentary tectonism. In: Dallmeyer, R.D. and Martínez García, E. (eds): Pre-Mesozoic Geology of Iberia, 334–347. Springer, Berlin.

Oliveira, J.T., Horn, M. and Paproth, E. (1979): Preliminary note on stratigraphy of the Baixo Alentejo Flysch Group, Carboniferous of Southern Portugal and on the palaeogeographic development, compared to corresponding units in Northwest Germany. Comunic. Serv. Geol. Portugal 65, 151–168.

Quesada, C. (1991): Geological constraints on the Paleozoic tectonic evolution of the tectonostratigraphic terranes in the Iberian Massif. Tectonophysics 185, 225–245.

Quesada, C. (1998): A reappraisal of the structure of the Spanish segment of the Iberian Pyrite Belt. Mineralium Deposita 33, 31–44.

Quesada, C., Fonseca, P.E., Munhá, J., Oliveira, J.T. and Ribeiro, A. (1994): The Beja-Acebuches Ophiolite (Southern Iberian Variscan fold belt) geological characterization and geodynamic significance. Bol. Geol. Min. España 105, 3–49.

Schermerhorn, L.J.G. (1971): An outline stratigraphy of Iberian Pyrite Belt. Bol. Geol. Min. España 82, 239–268.

Silva, J.B., Oliveira, J.T. and Ribeiro, A. (1990): South Portuguese Zone: Structural outline. In: Dallmeyer, R.D. and Martínez García E. (eds): Pre-Mesozoic Geology of Iberia 348–362. Springer, Berlin.

Surdam, R.C., Crossey, L.J., Hagen, E.S. and Heasler, H.P. (1989): Organic-inorganic interactions and sandstone diagenesis. Am. Assoc. Petrol. Geol. Bull. 73, 1–23.

Taylor, S.R. and McLennan, S.M. (1985): The continental crust: its composition and evolution, 312 pp. Blackwell, Oxford.

Thyne, G. (2001): A model for diagenetic mass transfer between adjacent sandstone and shale. Mar. Petrol. Geol. 18, 743–755.

Veblen, D.R. and Ferry, J. M. (1983): A TEM study of the biotite-chlorite reaction and comparison with petrographical observation. Am. Mineral. 68, 1160–1168.

Warr, L. and Nieto, F. (1998): Crystallite thickness and defect density of phyllosilicates in low-temperature metamorphic pelites: A TEM and XRD study of clay-mineral crystallinity-index standards. Can. Mineral. 36, 1453–1474.

Warr, L.N. and Rice, H.N. (1994): Interlaboratory standardization and calibration of clay mineral crystallinity and crystallite size data. J. Metamorphic Geol. 12, 141–152.

Yau, Y.-C., Peacor, D.R. and Essene, E.J. (1987): Hydrothermal treatment of smectite, illite and basalt to 460 °C: Comparison of treatment of natural with hydrothermally formed clay minerals. Clays Clay Mineral. 35, 241–250.

Manuscript received July 5, 2001; revision accepted June 18, 2002.
Editorial handling: S.Th. Schmidt